

電資學院外國學生專班

碩士學位論文

**A Study on Detection of Retinal Blood Vessels  
with their Geometrical Physical Characteristics  
for Retinopathy of Prematurity (ROP)**

研究生：**Ashish Kumar**

指導教授：**Prof. Yo-Ping Huang**

中華民國 110 年 7 月

# Abstract

Title: A Study on Detection of Retinal Blood Vessels with their Geometrical Physical Characteristics for Retinopathy of Prematurity (ROP)

Pages: 62

School: National Taipei University of Technology

Department: International Master of Electrical Engineering and Computer Science (IMEECS)

Time: July 2020

Degree: Master

Researcher: Ashish Kumar

Advisor: Prof. Yo-Ping Huang

Keywords: Retinopathy of prematurity (ROP), blood vessel segmentation, retinal fundus image, image processing.

In the human eyes, retinal diseases are correlated with the deformity present in the retina. These retinal diseases if not treated on time lead to vision loss and in some cases permanent blindness. In premature infants because of abnormal development of retinal blood vessels infants lose their eyesight. In clinical terms this disease is known as retinopathy of prematurity (ROP) and is one of the leading causes of irreversible blindness despite improvements in prevention over years. The regular vascular changes which occur at the back of the eye of an infant occur in a foreseeable manner after birth. Although in the past there are some solutions presented for early diagnosis of retinal diseases, most of the methods have been tested on publicly available datasets which have not found prolific in the diagnosis of ROP disease. Therefore, this study focuses on major problems in ROP

diagnosis that is the segmentation of retinal blood vessels in ROP fundus images followed by the length, width, and tortuosity measurement of the segmented blood vessels. Based on the results the ophthalmologist can perform an early diagnosis of ROP along with the approximate measurements of the vessels and reduce the probability of blindness occurs in infants. Firstly, for blood vessel segmentation in ROP images an image processing model was developed which consisted of noise reduction and contrast enhancement steps to overcome the low contrast, noise, and illumination problem. Secondly, we performed a delineation of morphological attributes of retinal blood vessels such as length, width, and tortuosity. For this centerline of vessels, branching point identification, endpoint identification, and automatic labelling of vessel segments were done using morphological operations and lookup tables. For vessel length measurement region property perimeter and geodesic distance transformation methods were compared. Finally, distance transformation was used for width measurement. Experiment results show that the proposed method outperformed the existing method for blood vessel segmentation in ROP images. Also, the method was effective in the measurement of morphological attributes of retinal vessels.

# **Dedication**

I dedicate my thesis to my mother Santosh Devi, my father Rakesh Kumar, my sisters Karuna Kumari and Priyanka Kumari, my brother in law Vikas Kumar, and my nephews Rudra and Nivaan.



# Acknowledgments

*Om Shri Ganeshaya Namah*

I would like to express my gratitude to *God*, who blessed me with this beautiful life and especially with the opportunity to study in National Taipei University of Technology, Taiwan. Guru Gobind Singh ji for his teaching that inspires me to do my best in becoming a kind person.

I sincerely thank Prof. Yo-Ping Huang for his guidance throughout my study in Taiwan and the opportunity to join his Ubiquitous Computing Lab. I thank him for believing in me, for always supporting me to do my best, for his professional advice, and for his kindness which inspires me to become a better person. It is truly an honor to become your pupil.

My special thanks go to my beloved parents and sisters, thank you for being a great source of love, inspiration, motivation, strength, and support. I might not be able to finish my study without their support, thank you.

Finally, and most I would thank to my lab mates and friends Kanika and Tanya for making my stay wonderful.

# CONTENTS

Abstract .....	i
Dedication .....	iii
Acknowledgments .....	iv
CONTENTS.....	v
List of Tables.....	vii
List of Figures .....	ix
Chapter 1 Introduction .....	1
1.2 Literature Review .....	3
1.3 Research Purpose .....	5
1.4 Limitations .....	5
1.5 Thesis Development .....	6
Chapter 2 Background .....	7
2.1 Classification of Retinopathy of Prematurity (ROP).....	7
2.2 Developed and Premature Retina .....	9
2.3 Retinal Imaging in Premature Infant's.....	10
2.4 Digital Image Processing .....	11
Chapter 3 Proposed Method .....	13
3.1 Dataset .....	15
3.2 Image Processing.....	16
3.2.1 Green Channel Extraction.....	16
3.2.2 Gray Scale Conversion .....	17
3.2.3 Contrast Enhancement .....	18
3.2.4 Background Noise Removal .....	19
3.2.5 Background Exclusion.....	20
3.2.6 Binarization.....	21

3.2.7 Morphological Opening.....	22
3.2.8 Smaller Components Removal .....	23
3.2.9 Outer Ring and Spur Removal.....	23
3.3 Length of Vessel Segments .....	24
3.4 Tortuosity and Width of Vessels Segments.....	29
Chapter 4 Experimental Results and Discussion .....	31
4.1 Retinal Vessel Segmentation Results.....	31
4.2 Branching Point Identification Results .....	35
4.3 Length, Width and Tortuosity Measurement Results.....	35
Chapter 5 Conclusions and Future Work .....	55
5.1 Conclusions.....	55
5.2 Future Work .....	56
References.....	57



# List of Tables

Table 1. Images sample.....	15
Table 2. Represents the length and width of vessel one for image 1.....	37
Table 3. Represents the length and width of vessel two for image 1.....	38
Table 4. Represents the length and width of vessel three for image 1.....	38
Table 5. Represents the length and width of vessel one for image 2.....	40
Table 6. Represents the length and width of vessel two for image 2.....	40
Table 7. Represents the length and width of vessel three for image 2.....	40
Table 8. Represents the length and width of vessel one for image 3.....	42
Table 9. Represents the length and width of vessel two for image 3.....	42
Table 10. Represents the length and width of vessel three for image 3.....	42
Table 11. Represents the length and width of vessel four for image 3.....	42
Table 12. Represents the length and width of vessel one for image 4.....	44
Table 13. Represents the length and width of vessel two for image 4.....	44
Table 14. Represents the length and width of vessel three for image 4.....	44
Table 15. Represents the length and width of vessel four for image 4.....	44
Table 16. Represents the length and width of vessel one for image 5.....	46
Table 17. Represents the length and width of vessel two for image 5.....	46
Table 18. Represents the length and width of vessel three for image 5.....	46
Table 19. Represents the length and width of vessel four for image 5.....	46
Table 20. Represents the length and width of vessel one for image 6.....	48
Table 21. Represents the length and width of vessel two for image 6.....	48
Table 22. Represents the length and width of vessel three for image 6.....	48
Table 23. Represents the length and width of vessel four for image 6.....	48
Table 24. Represents the length and width of vessel one for image 7.....	50



Table 25. Represents the length and width of vessel two for image 7.....	50
Table 26. Represents the length and width of vessel three for image 7.....	50
Table 27. Represents the length and width of vessel four for image 7.....	50
Table 28. Represents the length and width of vessel one for image 8.....	52
Table 29. Represents the length and width of vessel two for image 8.....	52
Table 30. Represents the length and width of vessel three for image 8.....	52
Table 31. Represents the length and width of vessel four for image 8.....	52
Table 32. Represents the length and width of vessel one for image 9.....	54
Table 33. Represents the length and width of vessel two for image 9.....	54



# List of Figures

Figure 1. Zones and stages of retinopathy of prematurity. (a) Diagram shows the retina in the right eye is divided into three zones. (b) Classification of retinopathy of prematurity: Stage 1, a thin demarcation line between vascularized and nonvascularized retina; Stage 2, a ridge; Stage 3, an extraretinal fibrovascular proliferation; Stage 4, partial retinal detachment; and Stage 5, total retinal detachment [31] .....	8
Figure 2. (a) Developed retinal image [32] and (b) Premature retinal image [33] .....	9
Figure 3. Flowchart of experiment method .....	13
Figure 4. Different channel images, (a) original RGB image, (b) red channel image, (c) green channel image, and (d) blue channel image.....	17
Figure 5. Gray scale images, (a) red channel, (b) green channel, and (c) blue channel ..	18
Figure 6. Contrast enhanced image.....	19
Figure 7. Histograms of, (a) green channel gray image and (b) contrast enhanced image .....	19
Figure 8. (a) Background mask and (b) new contrast enhanced image without background noise.. .....	20
Figure 9. (a) Average filtered image and (b) background excluded image.....	21
Figure 10. Binary image .....	22
Figure 11. Retinal vessel image after morphological opening .....	23
Figure 12. Clean image .....	23
Figure 13. (a) Network of vessels, (b) colored image, and (c) complemented image....	24
Figure 14. Canny edge detection .....	25
Figure 15. (a) Centerline of vessels, (b) centerline overlay on segmented image, and (c) centerline image overlay on enhanced image .....	26

Figure 16. (a) Dilated branch points and (b) branch points overlay on segmented image, (c) vessel centerline without branch point, and (d) discarded shorter segments ..	27
Figure 17. (a) Labelled vessel segment number 25, (b) morphological operation endpoint detection, and (c) lookup table endpoint detection .....	28
Figure 18. (a) Length of vessel segments using perimeter and (b) color map of geodesic distance transform.....	29
Figure 19. Width calculation using distance transform for vessel segment.....	30
Figure 20. (a) Input images and (b) vessel segmented images using proposed algorithm.. .....	33
Figure 21. (a) Input image, (b) T. L. Coye segmented image, and (c) Proposed method segmented image.....	34
Figure 22. (a) Input image and (b) branching points identified image .....	35
Figure 23. (a) Input image 1, (b) clean vessel image, (c) vessel segmented image with vessel labelled, (d) length of vessel segments using geodesic distance transform, and (e) tortuosity of vessel segments .....	37
Figure 24. (a) Input image 2, (b) clean vessel image, (c) vessel segmented image with vessel labelled, (d) length of vessel segments using geodesic distance transform, and (e) tortuosity of vessel segments .....	39
Figure 25. (a) Input image 3, (b) clean vessel image, (c) vessel segmented image with vessel labelled, (d) length of vessel segments using geodesic distance transform, and (e) tortuosity of vessel segments .....	41
Figure 26. (a) Input image 4, (b) clean vessel image, (c) vessel segmented image with vessel labelled, (d) length of vessel segments using geodesic distance transform, and (e) tortuosity of vessel segments .....	43

Figure 27. (a) Input image 5, (b) clean vessel image, (c) vessel segmented image with vessel labelled, (d) length of vessel segments using geodesic distance transform, and (e) tortuosity of vessel segments .....	45
Figure 28. (a) Input image 6, (b) clean vessel image, (c) vessel segmented image with vessel labelled, (d) length of vessel segments using geodesic distance transform, and (e) tortuosity of vessel segments. ....	47
Figure 29. (a) Input image 7, (b) clean vessel image, (c) vessel segmented image with vessel labelled, (d) length of vessel segments using geodesic distance transform, and (e) tortuosity of vessel segments .....	49
Figure 30. (a) Input image 8, (b) clean vessel image, (c) vessel segmented image with vessel labelled, (d) length of vessel segments using geodesic distance transform, and (e) tortuosity of vessel segments .....	51
Figure 31. (a) Input image 9, (b) clean vessel image, (c) vessel segmented image with vessel labelled, (d) length of vessel segments using geodesic distance transform, and (e) tortuosity of vessel segments .....	53

# Chapter 1 Introduction

In this chapter, a brief introduction about topic is given. Section 1.1 discusses about the motivation of study. Section 1.2 includes the literature review. Section 1.3 describes the research objective, Section 1.4 includes the limitations of this study, and Section 1.5 describes the thesis development.

## 1.1 Motivation

In human eye, retina is the inner layer of back of eye. Light enter through front of the eye and then focuses on retina. The retina then turns that light into visual message and then send message to brain to allow a person to see. In premature infants because of abnormal development of retinal blood vessels infants lose their eyesight. In clinical terms this disease is known as retinopathy of prematurity (ROP) and is one of the leading causes of irreversible blindness despite improvements in prevention over years. In premature-infants the retinal blood vessels are inchoate. Usually the infant is in mother's womb when the eyes finish developing because the child is not in the womb their growing environment is different so retinal blood vessels can grow abnormally.

Screening of a new-born baby for ROP is necessary if considered by his or her doctor to be at risk for ROP. Most infants who develop ROP will only develop a mild form of disease that will improve on its own without causing damage to the retina. Most babies for ROP will develop normal vision for their age but some infants will develop a severe form of ROP that can lead to a retinal detachment. A retinal detachment is when retinal becomes pulled away or separated from eye ball which can lead to permanent blindness. ROP remains one of leading cause of irreversible blindness worldwide despite the improvements in ophthalmic overhaul [1]. In U.S. there are approximately 3.9 million infants born each year. About 14,000 are affected by ROP and only 90% of those affected

will have mild disease that resolves on its own about 1,100 to 1,500 develop disease severe enough to require medical treatment. Despite advances in available medical treatment 400 to 600 infants each year become legally blind from ROP [2, 3]. Not all infants born prematurely are at risk for ROP those at highest risk for ROP are born before 31 weeks gestation or weigh 1,250 grams just under three pounds or less at birth. Typically all infants less than 31 weeks gestation or born weighing 1,500 grams 3.3 pounds or less undergo eye examinations to monitor for ROP [4].

Gestational age and birth weight are main risk factors for developing severe ROP. Other factors associated with presence of ROP include anaemia, supplemental oxygen, poor weight gain, poor overall health, prolonged mechanical ventilation, breathing difficulties, and blood transfusions [5]. While less common ROP can affect infants born at older ages and higher birth weights particularly if they have one more of these risk factors. Infants who are at risk for ROP are identified by a nurse or doctor in the neonatal intensive care unit (NICU). If an infant is at risk for ROP an ophthalmologist will perform a series of eye exams at repeated intervals to screen for ROP. An ophthalmologist is an eye physician who is skilled in the evaluation of infant eyes. Multiple eye exams are necessary because it cannot be predicted which babies will do well and which will develop problem. Eye exams need to be repeated until the retinal blood vessels have finished growing or the child is no longer at risk for ROP.

This thesis focuses on segmentation of retinal blood vessels in ROP fundus images followed by the length, width and tortuosity measurement of the segmented blood vessels. Based on the results the ophthalmologist can determine the stage of ROP along with the approximate measurements of the vessels and reduce the probability of blindness occurrence in infants.

## 1.2 Literature Review

Many researchers have shown their interest in conducting research in the field of biomedical imaging. It incorporates techniques for imaging different human organs which makes it more persuadable for continuing further analysis [6]. Taking in consideration human eye there are many problems which has been solved using the prior analysis. In all these retinal vessel segmentation for finding and combating the diseases has been a prominent task. In past different methods have been used for finding retinal vessels these include supervised, unsupervised, multi-scale, vessel tracking, mathematical morphology, thresholding based, model based and general approaches [7]. Fraz et al. [8] worked on an automated method for segmentation of retinal blood vessels. In which they used first order derivative of Gaussian filter, morphological top-hat transformation, and bit plane slicing. In another approach for segmenting blood vessels Fraz et al. [9] used first order derivative of Gaussian filter, morphological top-hat transformation, and region growing. Sigurosson et al. [10] developed an automatic retinal vessel extracting method based on path opening filter and fuzzy classification. Imani et al. [11] proposed improvement in blood vessel detection using morphological component analysis where for improving vessel map results they used separate lesions and morlet wavelet transform for enhancing blood vessels after which adaptive thresholding was employed to segment the retinal vessels. Roychowdhury et al. [12] proposed iterative vessel segmentation of fundus images where they used adaptive global thresholding for vessel segmentation purpose. Mapayi et al. [13, 14] introduced an adaptive thresholding technique for retinal vessel segmentation based on GLCM energy information. And also presented a comparative study of retinal vessel segmentation based on adaptive global thresholding, contrast limited adaptive histogram equalization and phase congruency. In this study for finding the blood vessels in retinal

images we used T. L. Coye algorithm [15] with modifications. This algorithm has been used previously in many related studies [16-20] for segmentation purpose.

Blood vessels play a significant role in identification of major diseases in eye like diabetic retinopathy, retinopathy of prematurity, hypertensive retinopathy, and degeneration of macula [21-24]. These diseases leads to changes in physical characteristics of blood vessels in eyes. Therefore, after vessel segmentation further analysis of vessels geometrical physical characteristics such as branching points, end points, bifurcation points, crossover points, centreline of vessels, length of each segments, length of each vessel, tortuosity of segments of vessels, vessel width, and width of each segment has become central ideal for ophthalmological medical applications. Grisan et al. [25] proposed a novel method for the automatic grading of retinal vessel tortuosity where they partitioned each vessel into segments of constant-sign curvature and then combine together each evaluation. Oloumi et al. [26] proposed diagnosis of plus disease in retinal fundus images via measurement of vessel tortuosity where they found that using median absolute deviation measure for detecting and remove linear parts improves accuracy for measuring tortuosity of vessels in comparison to their pilot study. Hao et al. [27] in their research measured vessel length in retinal vessel diameter measurement by using their proposed method to assess the diameter longitudinal change along the retinal vessel walls where their findings concluded that the longer length of measured vessel has less variation and provides a more reliable results. Kumar et al. [28] developed a technique was based on linear discriminative analysis which is an automatic method for computation of retinal blood vessels. Lowell et al. [29] proposed an algorithm for calculating blood vessel diameter to subpixel accuracy based on 2D difference of Gaussian model. Bhuiyan et al. [30] in their research proposed a method for detecting and classifying vascular bifurcation, branch, and crossover points based on the vessel



geometrical features. In this study we tried to incorporate all possible vessels geometrical physical characteristics necessary for retinopathy of prematurity which can help an ophthalmologist in performing timely treatment for an infant to prevent him/her from blindness.

## **1.3 Research Purpose**

This study proposes a method for retinal vessel segmentation in fundus images along with necessary geometrical physical characteristics in average for retinopathy of prematurity. We first segmented the retinal vessels from fundus images after which for finding the vessel length we found the centerline for our retinal vessel segmentation results and then divided them in small segments by removing the bifurcation and branch points. Then distance between each adjoining pair of pixels was calculated to found the length of each segments which was averaged out to find the total length of a vessel. We then calculated the distance between the endpoints for each segment of vessel and then these lengths were used for finding the tortuosity of each vessel segment. In last the width was computed for each segments by using distance transformation and extracting the distance along the centerline image which gave the radii. It was then doubled to found the width of vessels. By discovering all these geometrical physical characteristics about the retinal vessels in fundus images an ophthalmologist can perform timely treatment for an infant to prevent him/her from blindness.

## **1.4 Limitations**

There are several limitations in this study, such as:

1. This study focus on detection of retinal blood vessels along with vessels geometric physical characteristics for retinopathy of prematurity images.

2. This study used images positive for retinopathy of prematurity as an input.
3. This study used image processing techniques for detection and determination of retinal blood vessel and geometrical physical characteristics of retinal vessels.
4. The proposed method will no longer properly detect the physical characterizes of vessels if the retinal vessels are not clearly segmented due to noise in images. As the noise in input images increase the pixel values for segmented image might be different. Hence, the retinal vessel detection becomes difficult.
5. The input images for vessel segmentation require more preprocessing steps for noise free images.

## **1.5 Thesis Development**

The structure of the remainder of this thesis is outlined below.

- Chapter 2 introduces the concept of major techniques.
- Chapter 3 describes the detail process of this experiment.
- Chapter 4 presents the results and discussion.
- Chapter 5 presents the conclusions.

## Chapter 2 Background

In this chapter, a brief background is given. Section 2.1 introduces classification of ROP. Section 2.2 gives the explanation about developed and premature retina. In section 2.3, retinal imaging in premature infants is described and section 2.4 gives a brief explanation about digital image processing.

### 2.1 Classification of Retinopathy of Prematurity (ROP)

The international classification of retinopathy of prematurity (ICROP) is the system that provides direction for classification of ROP [1]. When an ophthalmologist looks inside an infant's eyes or photographs of retina they evaluate the level of development of retina. They evaluate various parameters while looking in infant's eyes these are disease location or zone of growth i.e. how far the blood vessels have grown, disease severity or stage of disease and appearance of blood vessels whether they are thick or wavy for determination of plus disease.

Retinal development is describe by three zones. Zone I is the least developed and Zone III is the most developed. Retinal vessels that have grown far and remain in Zone I are the least developed. As the retina develops the retinal blood vessels grow out from Zone I and enters in Zone II and as retina continues to develop the retinal blood vessels grow into Zone III. Once retinal blood vessels have grown into edge of Zone III they are finished growing and the retina is considered fully developed. If ROP is present ophthalmologist will describe the severity of ROP as stage of ROP. There are five stages of ROP. The premature retina is considered as stage 0 of ROP which is the least severe stage whereas stage 5 is the most severe stage. Figure 1 describes the stages of ROP.

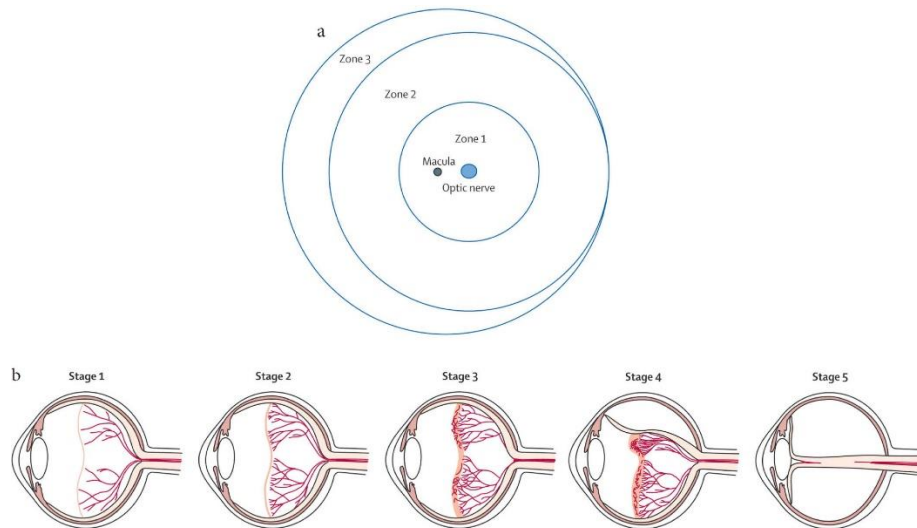


Figure 1. Zones and stages of retinopathy of prematurity. (a) Diagram shows the retina in the right eye is divided into three zones. (b) Classification of retinopathy of prematurity: Stage 1, a thin demarcation line between vascularized and nonvascularized retina; Stage 2, a ridge; Stage 3, an extraretinal fibrovascular proliferation; Stage 4, partial retinal detachment; and Stage 5, total retinal detachment [31].

- Stage 1 is a faint demarcation line. This is considered as mild disease where abnormal vessel growth is seen. Many infants who develop this improves with no treatment and eventually develop normal vision.
- Stage 2 is an elevated ridge. This is considered as moderate disease where moderately abnormal vessel growth is seen. This disease resolves on its own without further progression.
- Stage 3 is when fibrovascular tissue gets extraretinal. This is considered as severe disease where severely abnormal vessel growth is seen. Vessels rather than growing normally along the surface of retina they began to grow above retinal surface. These abnormal blood vessels are leaky and can cause bleeding within the eye. When an infant suffers from certain degree of Stage III and plus disease develops, then treatment is considered. In plus disease the blood vessels of the retina become enlarged and twisted.

- Stage 4 is partial retinal detachment. Here the abnormal blood vessels cause the retina to be pulled away or detach from the wall of the eye known as retinal detachment. Despite accurate diagnosis and timely treatment the ROP sometimes continues to worsen and retina can detach. In this only a part of retina is detached from eyeball.
- Stage 5 is the total retinal detachment. This is considered as most severe disease. Eyes with retinal detachment caused by ROP generally have poor visual outcome.

## 2.2 Developed and Premature Retina

In this study, we have used premature retinal images rather developed retinal images. In premature retinal images vessel segmentation is a challenging task. As the retinal vessels in premature retinal images do not grow fully and stop growing after a certain time where as in developed retinal images the retinal blood vessels growth could be seen as vessels reach the edges of the image. Figure 2 demonstrate an example of a developed and premature retinal image where (a) is a color fundus photograph of a 35 year old healthy patient. The media are clear, providing a crisp view of the fundus and (b) a fundus photograph to show immature retinal vascularization. The arrows show the progressive tapering of retinal vessels.



Figure 2. (a) Developed retinal image [32] and (b) Premature retinal image [33].

Vessel segmentation in fundus images also depends on different factors such as clarity of images, the amount of noise in images and the clarity of vessels in the images. Although there are different image filtering and contrast enhancement techniques but not all works sometimes on premature retinal images as the vessels are fragile and not fully grown. It sometimes becomes difficult for even human eyes to identify the retinal blood vessels in fundus images. Hand labelling for ground truth of vessels is also difficult and require guidance from an experienced ophthalmologist.

## **2.3 Retinal Imaging in Premature Infant's**

Retinal imaging entails generating a two-dimensional (2D) image of the three-dimensional (3D) retinal tissue obtained using the reflected light. This retinal imaging technique is considered essential for management and diagnosis of disease processes in ophthalmic practice. Therefore, retina fundus imaging can be described as a process which results in a 2D image where the image intensities represent the amount of a reflected quantity of light. There are different techniques which belong to fundus imaging these include fundus photography or red-free photography, color fundus photography, hyper spectral imaging, scanning laser ophthalmoscopy (SLO), adaptive optics SLO, stereo fundus photography, and fluorescein angiography and indocyanine angiography [34]. Retinal imaging techniques have evolved at a remarkable pace in the last few decades this is because of the reason that it is a simple technique to master and helps doctors to cover large retinal fields at a given time for diagnosis of diseases. The recent developments which lead to Wide field imaging (WFI) and ultra-wide field imaging (UWFI) are now increasingly popular.

In order for insides of eye to be examined by an ophthalmologist eye drops are placed in an infant's eye to dilate or enlarge the black spot present in center of the eye known as

pupil. When the pupil is dilated the ophthalmologist are able to look at back of infant's eyes for examination of retina. During the examination infants are positioned and made comfortable by methods such as swaddling with blankets and sometimes given sugar solution by mouth or a pacifier. Instruments are used to hold the eyes open and move the eye during examination a numbing drop is placed prior to this. An eyelid speculum is generally used to hold the eyelids open.

The ophthalmologist use special equipment to examine the inside of the eye this equipment has a bright light which allows the ophthalmologist to examine the retina, a camera may also be used to photograph the retina. This special equipment to examine the inside of eye is known as indirect ophthalmoscope, which has a special lens that sends a bright light into the eye, enabling the doctor to examine the retina. A scleral depressor is an instrument which helps move the eye into different positions so the entire retina can be checked. There are ongoing researches being performed for evaluating the efficacy of digital photography for diagnosing ROP. Doctors nowadays are using an innovative device called the RetCam, a special camera that takes high-resolution digital pictures of the retina. It provides detailed images that can be compared from one exam to the next to help track the health of infant's eyes over time.

## 2.4 Digital Image Processing

An image can be described as two dimensional (2D) function  $f(x,y)$ . The amplitude of  $f$  at any pair of coordinates  $x,y$  is called the *gray level* of the image at that point. Digital image is where the value of  $x,y$  and  $f$  is finite. An element within a digital image is called "pixel". Digital image processing refers to processing digital images by means of a computing device such as PC.

There are three types of computerized processes, i.e. low-level process, mid-level process, and high-level process. Low-level process involve operation such as image processing to reduce noise, contrast enhancement, and image sharpening. Mid-level process involve task such as segmentation or classification. High-level process involves “making sense” of an ensemble of recognized object.

Several image processing tasks such as image filtering, contrast enhancement, noise removal, thresholding, and labelling have been used in this study. Since image are defined into two dimensions (perhaps more), any information obtained in each process can be further processed according to user needs. Especially in this study, the information obtained in each process is processed in such a way to obtain the desired results. The technique we used will be more explained in Chapter 3.





## Chapter 3 Proposed Method

In this chapter, methods will be discussed in detail. For the image processing we apply MATLAB as the development environment. Figure 3 shows the flowchart of method used for detection of retinal vessels and calculation of vessel geometrical physical characteristics.

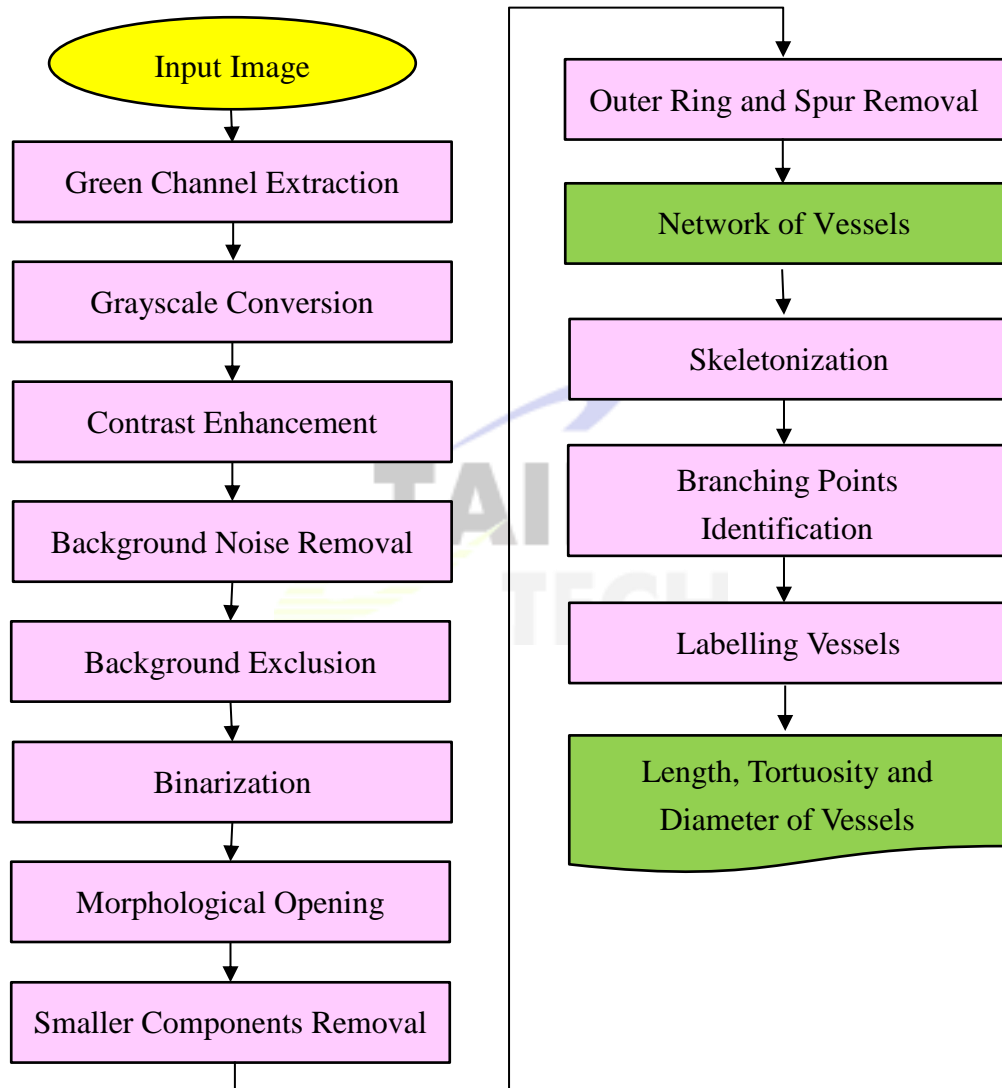


Figure 3. Flowchart of experiment method.


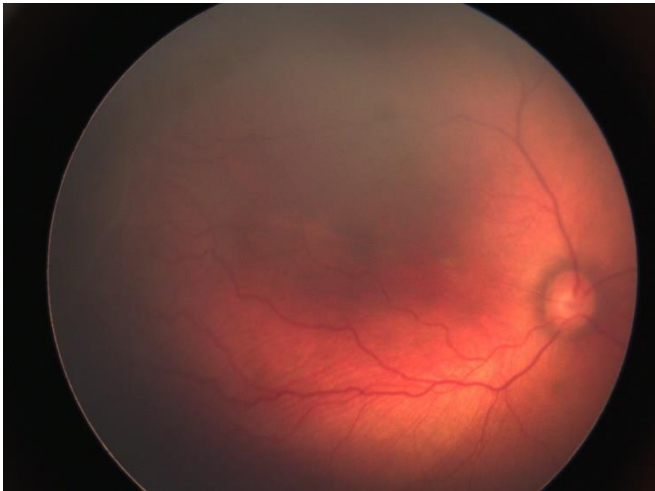
The proposed method for extracting the network of vessels consist of nine steps. The first step is green channel extraction, the purpose of this step is to extract the channel from input image which gives better contrast. The second step is grayscale conversion. This is

done to convert the green channel colored image into gray scale image where principal component analysis (PCA) of weighted lab model is used. The third step is contrast enhancement. This step further enhances the contrast of gray scaled image by using contrast-limited adaptive histogram equalization (CLAHE) for obtaining highlighted vessels in image. The fourth step is background noise removal. The boundary mask image is made which is used to remove the background noise in the image. The fifth step is background exclusion. The enhanced image is further filtered to remove noise in image and this filtered image is used to exclude the background. The sixth step is binarization. This step requires a fair threshold value to get a decent thresholding image for binarization process. The seventh step is morphological opening used for removing smaller objects (noise) while preserving shape and size of larger objects. The eighth step is outer ring and spur removal which is done to remove the outer ring in fundus image followed by removal of small spurs attached to retinal vessels for obtaining clean vessels image. The final step for obtaining network of vessels requires removing smaller components (further noise) present in image. For further delineation of morphological attributes of retinal blood vessels five steps are performed. The first step is skeletonization for obtaining the centerline of vessels. The second step is branching points identification where branching, bifurcation and crossover points are identified and removed from images for obtaining vessel segments for finding length. The third step is labelling of vessels where the shorter segments are automatically labelled. The fourth step is finding length of shorter segments. In this length of every segment is computed and averaged out for finding average length of vessel. The fifth step is tortuosity of vessels. The purpose of this step is to find the twistedness of every segment of vessel. The final step is to find the width of vessels which requires computing width of every segment using distance transformation for finding average width of vessel.

### 3.1 Dataset

The dataset we used in this study is premature retinal images having ROP provided by Chang Gung Memorial Hospital in Taipei, Taiwan. We used nine images in our research. The images are in RGB format with 1600×1200 pixel size per image. Table 1 shows two examples of images used in this study. The dataset consist of both OS (oculus sinister) means left eye and OD (oculus dextrus) means the right eye images.

Table 2. Images sample.

Images	Image display	Image properties
Image 1		Format: RGB
		Extension: JPG
		Size: 1600×1200 pixel
		Bit depth: 24 bit
		Resolution: 300 dpi
Image 2		Format: RGB
		Extension: JPG
		Size: 1600×1200 pixel
		Bit depth: 24 bit
		Resolution: 300 dpi

## **3.2 Image Processing**

In this section we introduce an image processing technique for retinal vessel segmentation and delineation of morphological attributes of retinal blood vessels. The technique involves green channel extraction, gray scale conversion, contrast enhancement, background noise removal, background exclusion, binarization, morphological opening, outer ring with spur removal, shorter components removal, skeletonization, branching point identification, labelling of vessels, vessels length, width, and tortuosity in pixels.

### **3.2.1 Green Channel Extraction**

In general the premature retina fundus images is an RGB colored image which consist of three channels that are red, green and blue channel. Not all the channels comprise of clear vessels for image segmentation purpose we investigated the proper channel selection in this study for localization purpose of the retinal blood vessels. This was accomplished by separating the input image into channels and using one of them as input for vessel detection. The blue channel image was found to be of low contrast and doesn't have much retinal vessels. The red channel image was found to be of fair contrast but since most of features were emitting a signal in red channel image and too much noise was present it was not chosen. Finally, the green channel image was selected as it provided an adequate contrast with darker retinal blood vessels on brighter background visible with normal sight. Figure 4 shows different channel images.

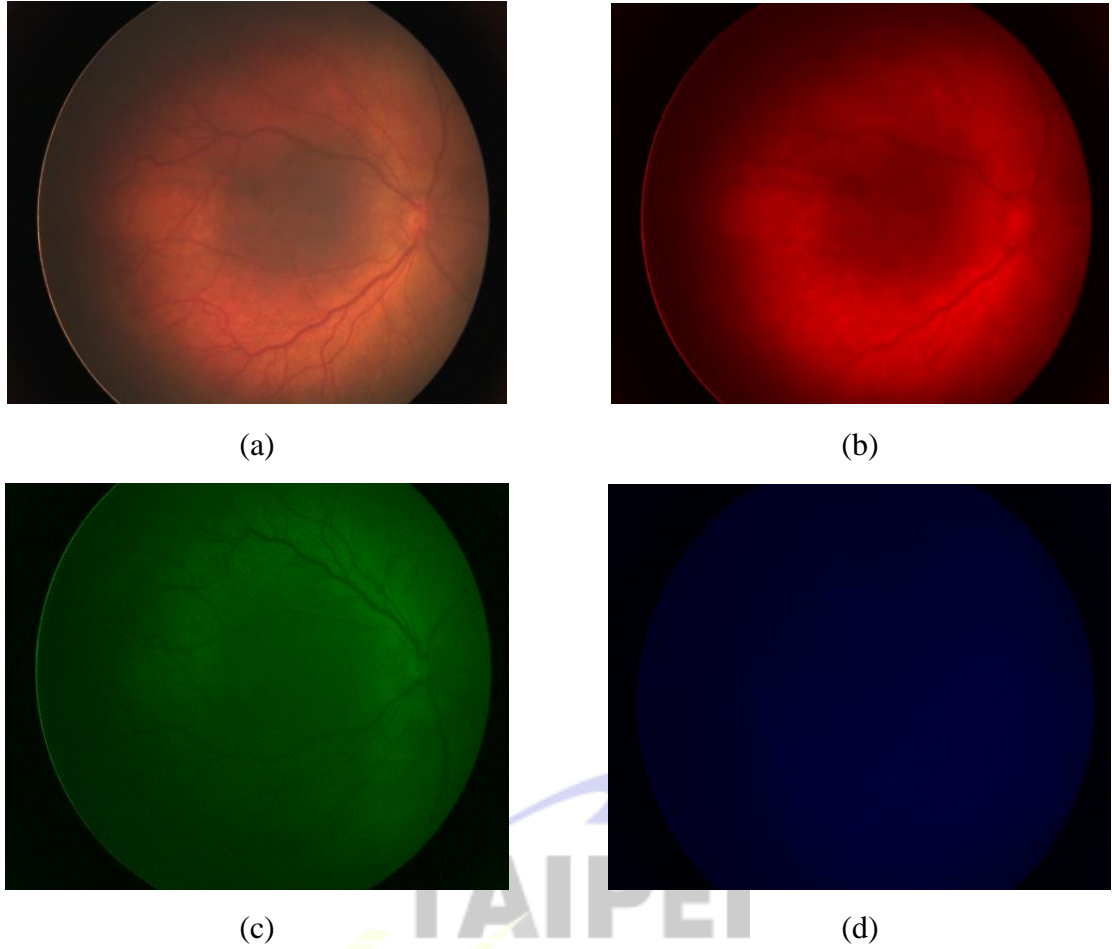


Figure 4. Different channel images, (a) original RGB image, (b) red channel image, (c) green channel image, and (d) blue channel image.

### 3.2.2 Gray Scale Conversion

Before converting the green channel image to gray scale we resized the input green channel image to  $584 \times 565$  to make computation faster as original image was very big. The original pixel values in image were in integers which cannot accept decimal points. For segmentation of blood vessels we needed precession till decimal points so we convert resized image into double data type after which the conversion was performed in lab color space [35]. Then the principle component analysis (PCA) of weighted Lab color model is used for converting the image into grayscale. Figure 5 shows the gray scale images of red, green and blue channel where the vessels

presence can be seen more clearly in green channel image.

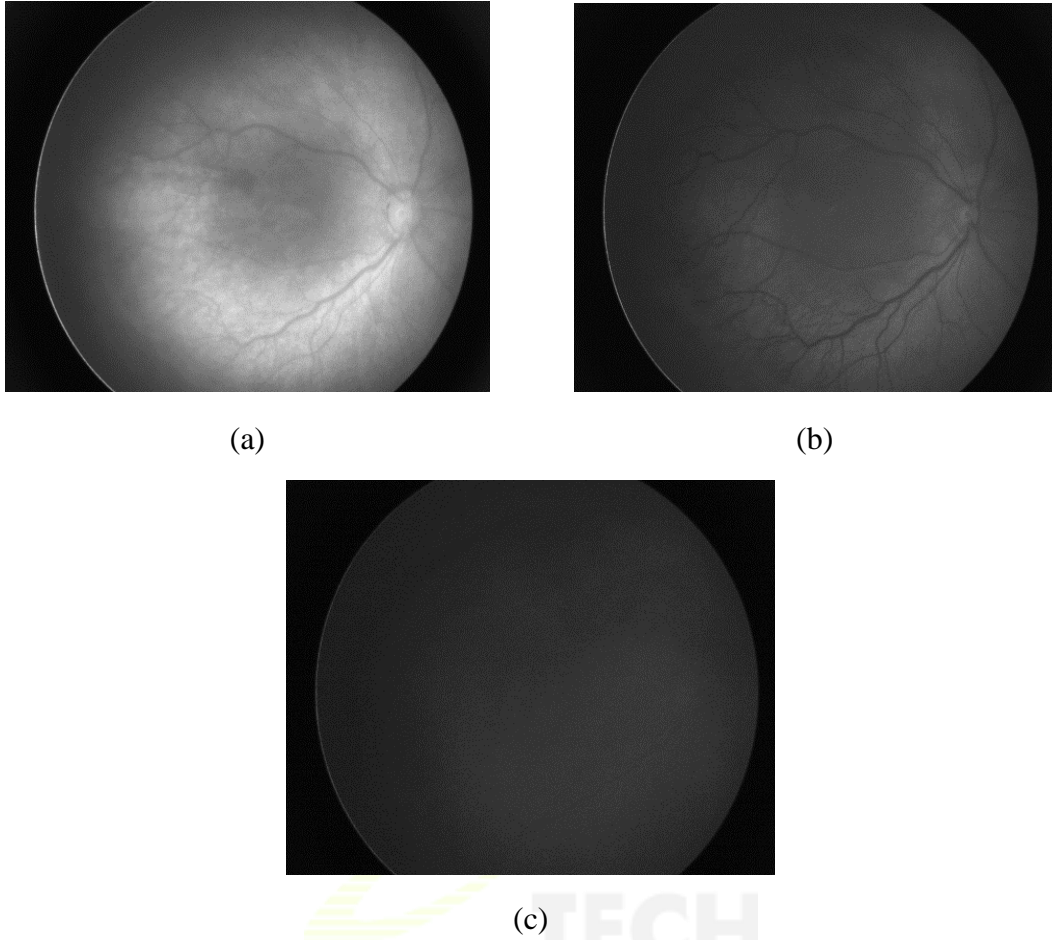


Figure 5. Gray scale images, (a) red channel, (b) green channel, and (c) blue channel.

### 3.2.3 Contrast Enhancement

On the green channel gray scale image we performed contrast enhancement by using contrast-limited adaptive histogram equalization (CLAHE). In standard adaptive histogram equalization (AHE) noise present in image also gets amplified so to prevent this we used CLAHE in this study. In contrary to AHE, CLAHE works on smaller regions present in the image which are known as ‘tiles’. Each tile contrast is enhanced by using this equalization technique resulting in a histogram of output region which approximately match a specified histogram. In histograms bin is greater than the described contrast limit

then those pixels are clipped and distributed to other bins uniformly before AHE. For annihilating artificially induced boundaries CALHE combines the neighboring tiles using bilinear interpolation [36]. The tile size was chosen to be  $8 \times 8$  and total number of bins selected were 128 for experimental purpose. Figure 6 shows the contrast enhanced image and figure 7 shows the histograms of green channel gray image and contrast enhanced image which clearly shows how the intensity was increased and decreased in some regions.



Figure 6. Contrast enhanced image.

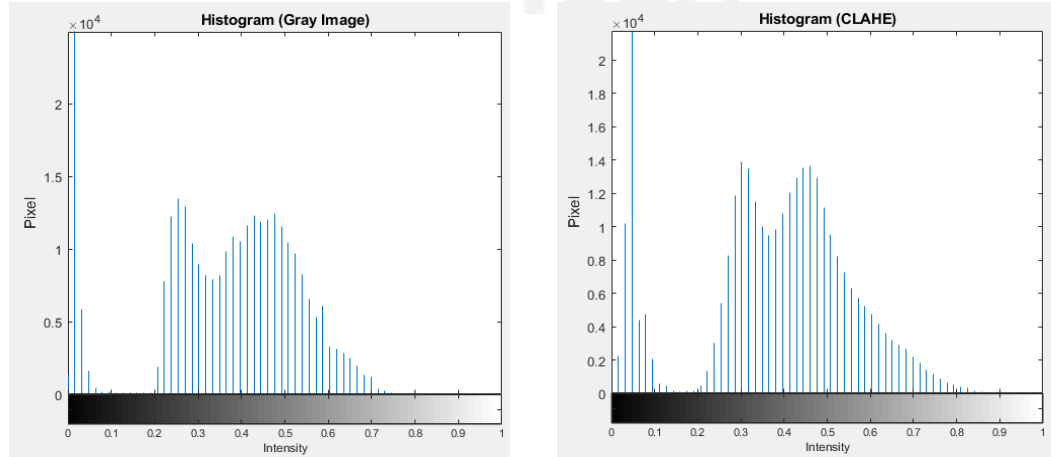


Figure 7. Histograms of, (a) green channel gray image and (b) contrast enhanced image.

### 3.2.4 Background Noise Removal

The contrast enhanced image had background noise in it which was visible in the

image for removing this we performed background noise removal by creating the mask of input image. For creating the mask of input image we performed binarization operation for converting the 2D contrast enhanced image to grayscale. Then we filled in the holes present in the image followed by removing smaller objects less than 100 pixels in the converted binary image. Finally, the subtraction of this masked image was performed on the contrast enhanced image to generate a new contrast enhanced image. Figure 8 shows the background mask and new contrast enhanced image without background noise.

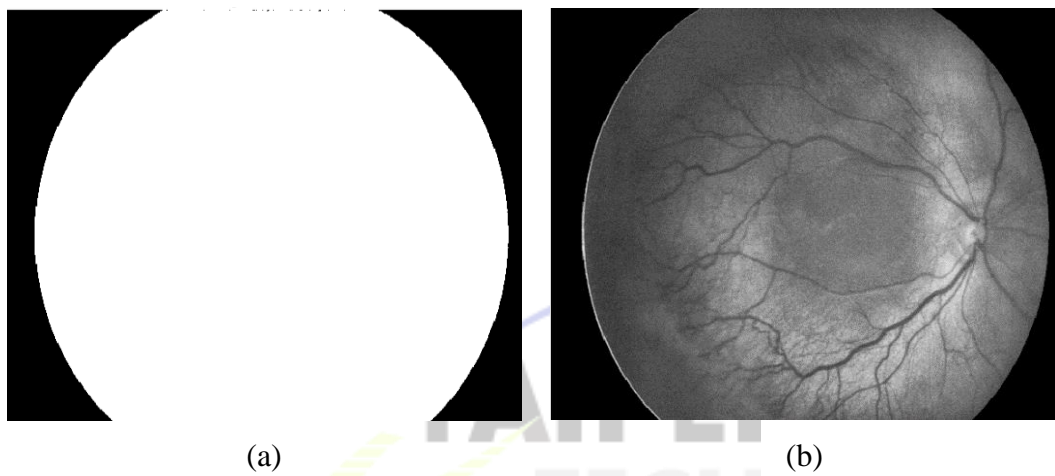


Figure 8. (a) Background mask and (b) new contrast enhanced image without background noise.

### 3.2.5 Background Exclusion

After obtaining the new enhanced image background exclusion was performed on it. For this we employed an image filtering technique. Image filtering is used for highlighting certain features or removing certain features in images. In this study, we used a spatial domain filter, average filter, for removing the noise in the inner region of fundus image. The average filter works by moving through the image pixel by pixel replacing each value with the average of value of neighboring pixels including itself [37]. The size of average filter used was  $10 \times 10$  for experiment purpose. After which the background was excluded by subtracting the average filtered image from the new enhanced image. Figure 9 shows



the average filtered image and background excluded image.

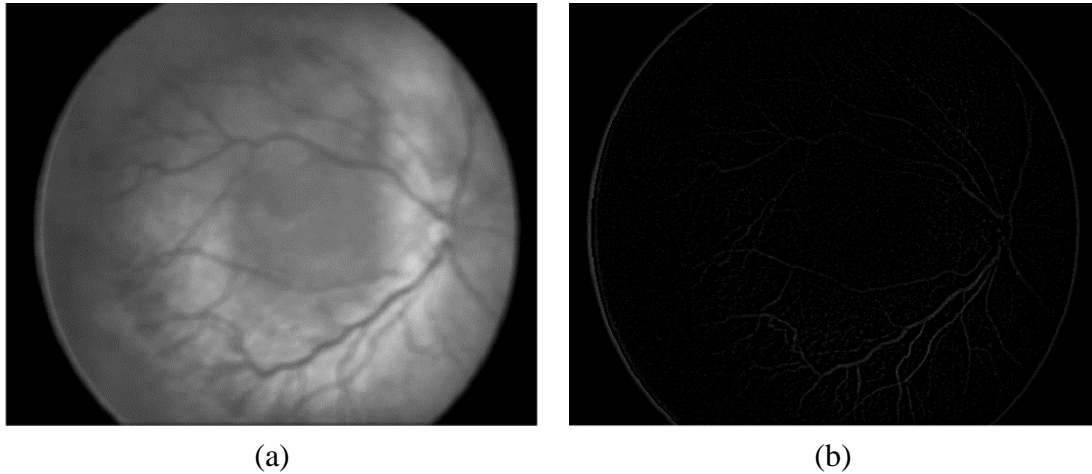


Figure 9. (a) Average filtered image and (b) background excluded image.

### 3.2.6 Binarization

On the background excluded image binarization was performed to obtain the binary image for finding the retinal blood vessels in the image. To obtain the vessels from the background excluded image, a proper threshold value need to be determined. For determining the threshold value ISODATA [38] method was used. The ISODATA method computes a global image threshold by using iterative isodata method. This method assists in producing a global threshold i.e. level which was used for converting the intensity image to a binary image. The derived level value is normalized intensity value and lies between 0 and 1. Initially the histogram was segmented into two regions where a starting threshold value which is half of maximum dynamic range is selected. The sample means of the gray values associated with the background and foreground pixels were computed. Then new threshold value was computed as average of these two sample means. The process repeated until the threshold value does not change any more. While converting the image to binary image the level was reduced by 0.008 and then binarization was performed. Figure 10 shows the binary image.

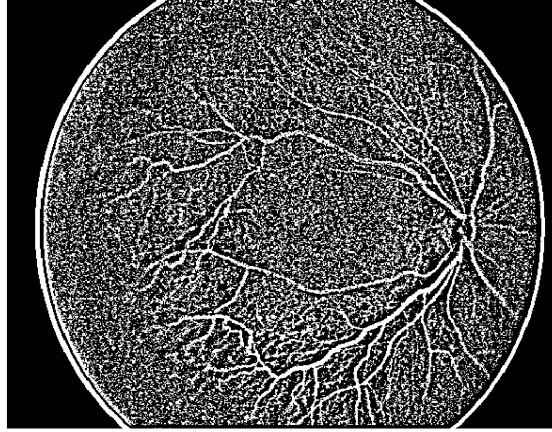


Figure 10. Binary image.

### 3.2.7 Morphological Opening

After the binarization operation the retinal blood vessels present in the image were classified as white and the background was classified as black. For further removing the noise present in the inner region where the vessels are present we performed morphological operation named opening. This noise present in the inner region is also white i.e. why the structural differences between the noise present in image and retinal blood vessels are examined. Morphological opening helps in removing these noises while preserving the vessels which were not in contact with the noises. Morphological opening is a combination of two morphological operations named erosion and dilation [39]. A disk-shaped structuring element with a radius of 1 pixel was created and opening operation was performed with help of this structuring element. Figure 11 shows the retinal vessel image after morphological opening.

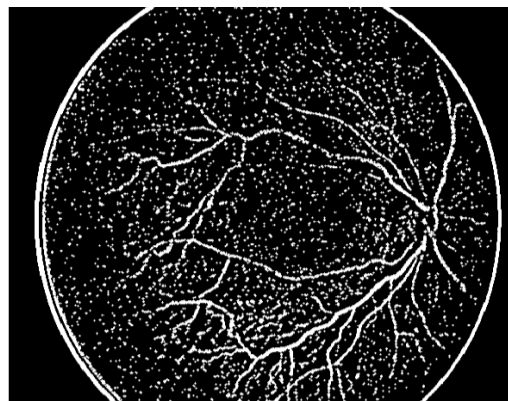


Figure 11. Retinal vessel image after morphological opening.

### 3.2.8 Smaller Components Removal

The retinal vessel image after morphological opening was further cleaned to find out the vessels present in the image which did not come in contact with noise. For removing the smaller noise still present in image we performed area opening [15]. After different values were tested the maximum number of pixels in object was specified as a nonnegative integer value. It helped in removing all noises that are fewer than 90 pixels from the vessel image after morphological opening producing image with clean vessels.

Figure 12 shows clean vessel image.

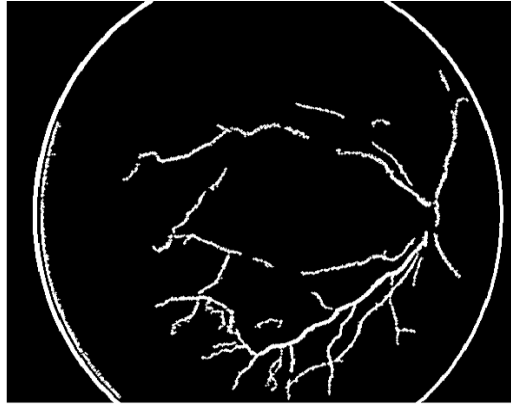


Figure 12. Clean image.

### 3.2.9 Outer Ring and Spur Removal

For finally extracting the network of vessels outer ring and spur present in the image were removed. The outer ring formed in fundus images is because of the limits of the fundus cameras. For removing the outer ring we used the masked image and removed the inner region out from the clean image. After which spur removal was done. Spurs are unwanted parasitic components, these appear in retinal vessel segments and are not key to the retinal vessel segments [37]. Figure 13 shows the network of vessels. The input

fundus image has a reflection in it because of which the circle lining after outer ring removal is present in figure 13.

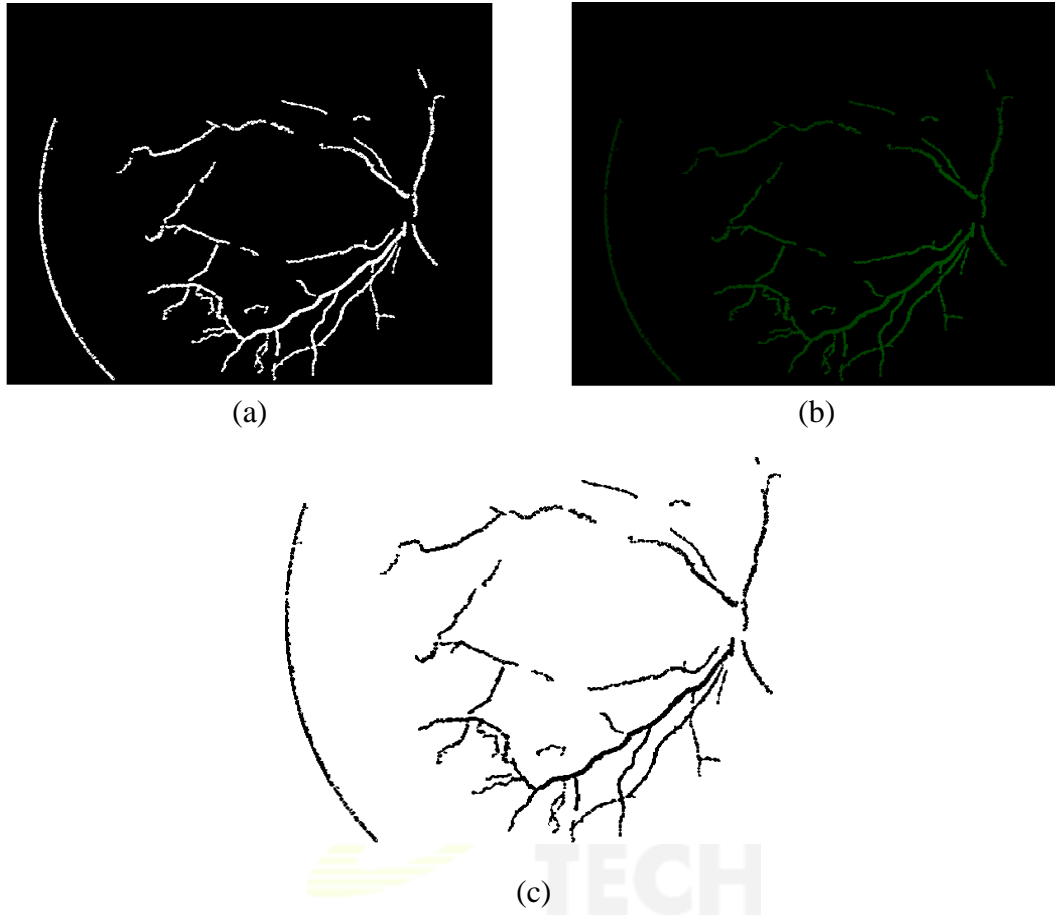


Figure 13. (a) Network of vessels, (b) colored image, and (c) complemented image.

### 3.3 Length of Vessel Segments

After we obtained the network of vessels we performed a certain set of operations to find the length of vessels. For these edges of vessels, centerline of vessels (skeletonization), branching point identification, vessel labelling and endpoint detection was done. Firstly we performed edge detection on images to find out the edges of the retinal vessels and to separate different objects like the optic disk if found in images. We used different edge detection techniques named canny, prewitt, roberts, log, zerocross, approx-canny, and sobel. It found out that canny edge [40] detected result was found to

be the cleanest as it was able to find out all edges from the vessel segmented image. Canny edge detection works in five steps after image acquisition it smoothens the image by convolving with gaussian filter then computes the gradients where edges are marked where gradient of image is large followed by non-maximum supervision where local maxima is marked as edge and hysteresis thresholding which determines the final edges by suppressing all edges which are not to a very strong edge. Figure 14 shows canny edge detection of retinal vessels.

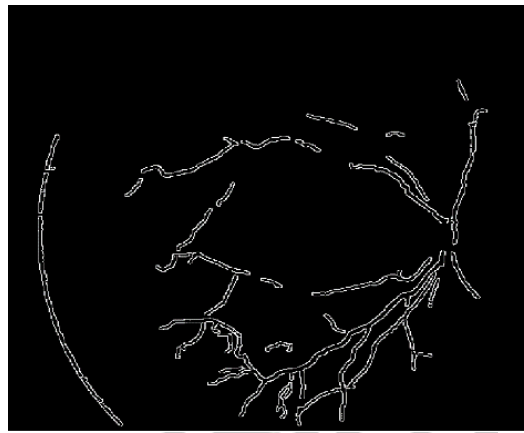


Figure 14. Canny edge detection

Then the centerline of vessels was found out using morphological operation skel [41]. It removes pixels on the boundaries of objects preventing objects from breaking apart. The remaining pixels then make up the image showing the centerline of vessels. The centerline of vessels was overlaid on segmented image and enhanced image for clear visualization of vessel centerline and not identified thin vessels. Figure 15 shows (a) centerline of vessels (b) centerline overlay on segmented image (c) centerline image overlay on enhanced image which shows the very thin vessels at end were not identified.

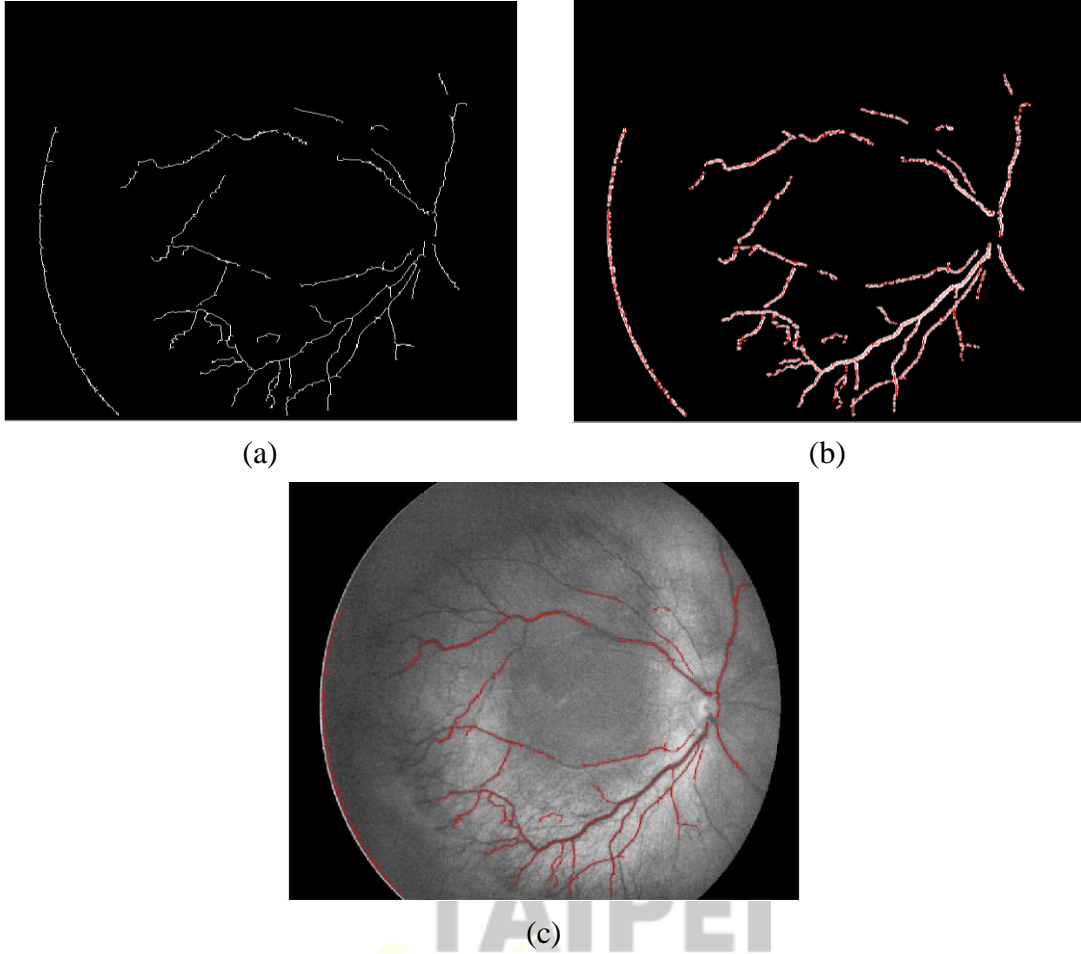


Figure 15. (a) Centerline of vessels, (b) centerline overlay on segmented image, and (c) centerline image overlay on enhanced image.

Retinal blood vessels tend to grow non-uniformly and have no bifurcations as it grows larger. For the purpose of measuring the length of vessel segments automatically and finding diameter of vessel segments in further steps branching point identification [41] and removal was done. The retinal blood vessels tend to appear thicker at branching points when there is bifurcation of edges. Therefore, we removed the branching points from the vessels. This was done in three steps. Firstly we identified the branching points using morphological operations. Some of the missing pixel regions were also included as branching points. We then dilated the branching points identified and overlaid on vessel segmented images to clearly identify the missing pixel and bifurcation points. Secondly these branching points were removed from the centerline image to obtain an image without branching points. Thirdly, shorter segments below 15 pixels were discarded to

obtain only bigger vessels for labelling purposes and calculation of length of vessels. Figure 16 shows (a) Dilated branch points (b) branch points overlay on segmented image (c) vessel centerline without branch point (d) discarded shorter segments.

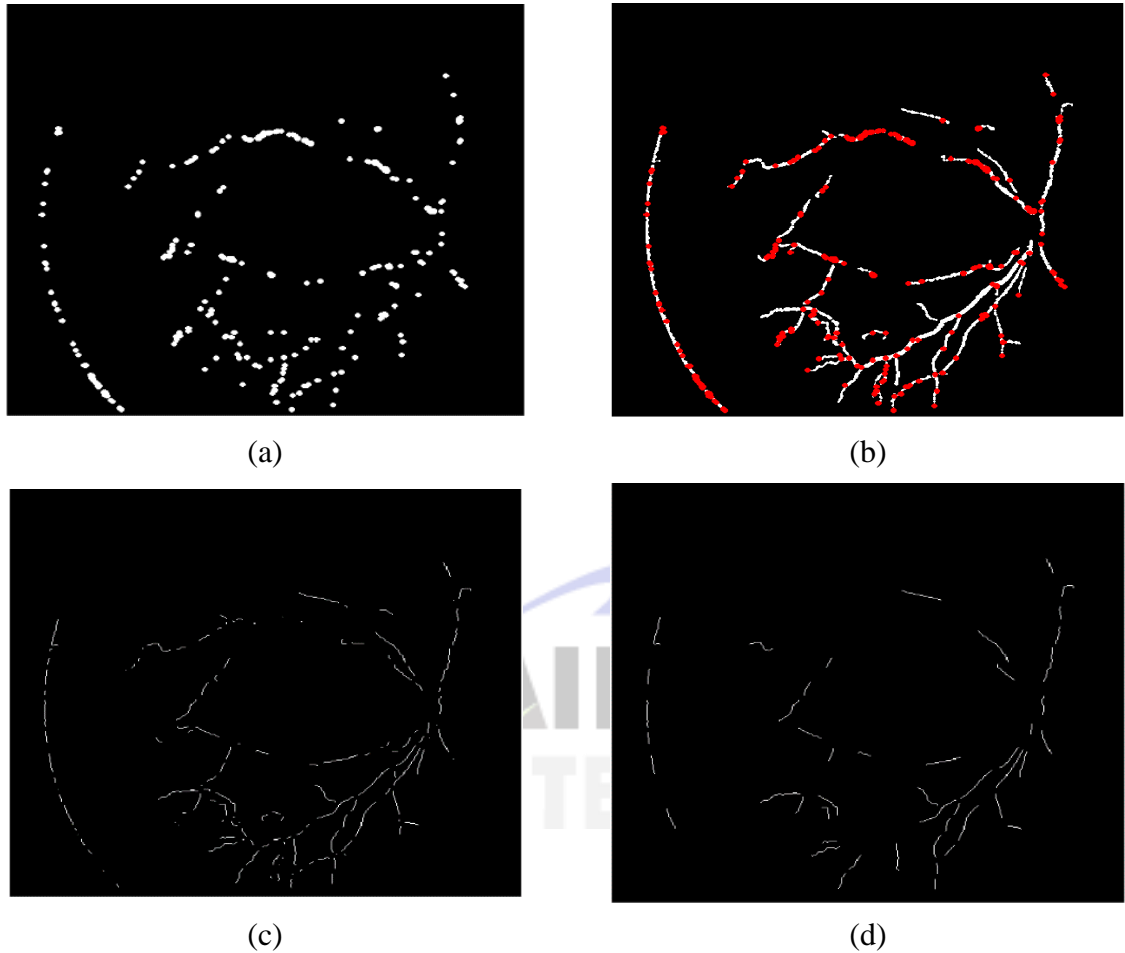


Figure 16. (a) Dilated branch points, (b) branch points overlay on segmented image, (c) vessel centerline without branch point, and (d) discarded shorter segments.

Labelling and dilation of vessel segments [41] were performed next. Automatically labelling for connected components in image was done. Label returns the label matrix  $L$  that contains labels for the 8-connected objects found in image. The pixels are said to be connected if their edges or corners touch. Two adjoining pixels are considered part of the same object if they are both on and are connected along the horizontal, vertical, or diagonal direction. Then endpoint detection was performed using two different methods as we used two different approaches for finding out the length of vessel segments. The

endpoint detection was done using morphological operation on binary images [41] and using lookup tables. A lookup table is generally a column vector in which every element represents the value to return for one possible combination of pixels in a neighborhood. For example in a  $3 \times 3$  neighborhood if central pixel is one and if exactly there is one more pixel one in the neighborhood then central pixel is considered as endpoint. Figure 17 shows (a) labelled vessel segment number 25 (b) morphological operation endpoint detection (c) lookup table endpoint detection. Both the techniques were successful in endpoint detection.

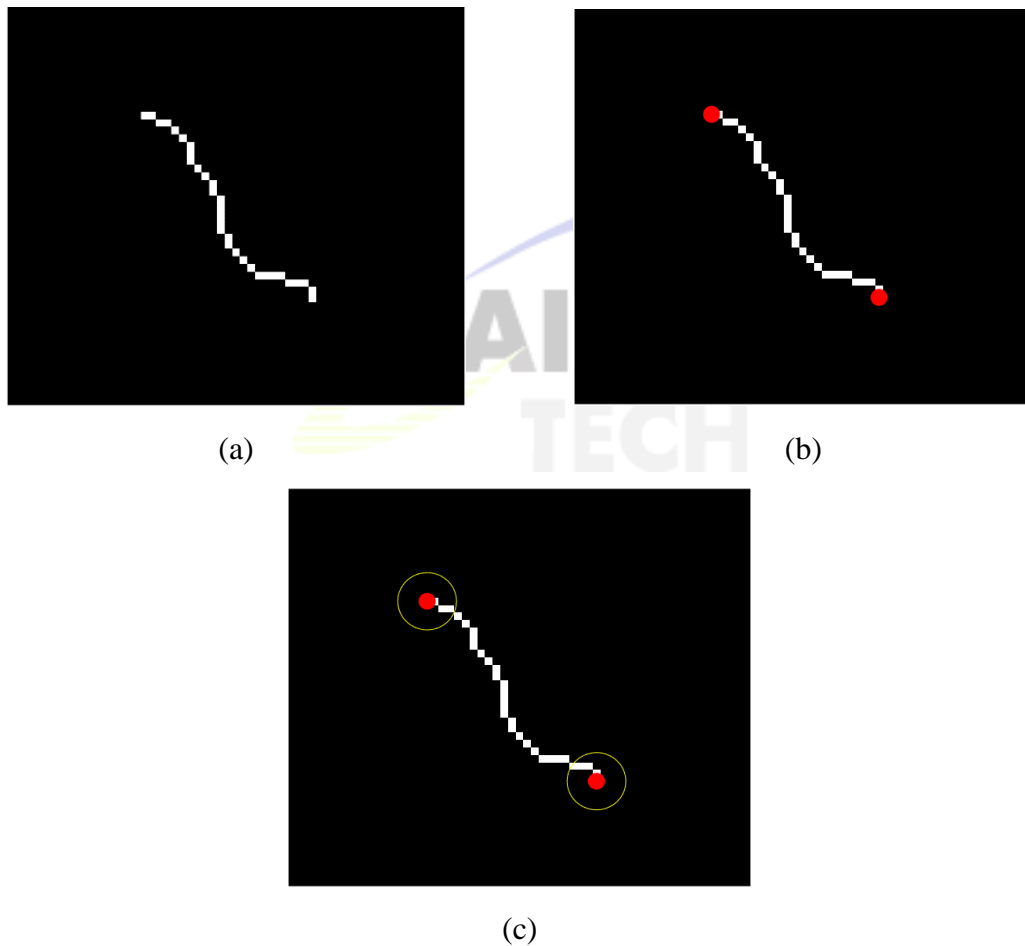


Figure 17. (a) Labelled vessel segment number 25, (b) morphological operation endpoint detection, and (c) lookup table endpoint detection.

We used two methods for finding the length. For the first method we used endpoints found using morphological operations and region properties for measuring properties of



image regions where perimeter was used as a property. Perimeter calculates the distance around the boundary of the region which is then returned as a scalar. The perimeter was computed by calculating the distance between each adjoining pair of pixels around the border of the region. Prior to the discontinuous regions in image were removed keeping the longer segments only for preventing the model from returning any unexpected results. For the secondly method we used endpoints found using lookup tables and geodesic distance transform [42]. It calculates the distance between any true pixel in an image and constraint nearest non zero pixel. It means if we have two pixels next to each other the constraint is we cannot jump over a black region. The color map in Figure 18 (a) shows the length of vessel segments result using perimeter property and (b) shows color map traversing from starting point to end the geodesic distance transform gets successfully larger and maximum value at end gives measure for length of path.

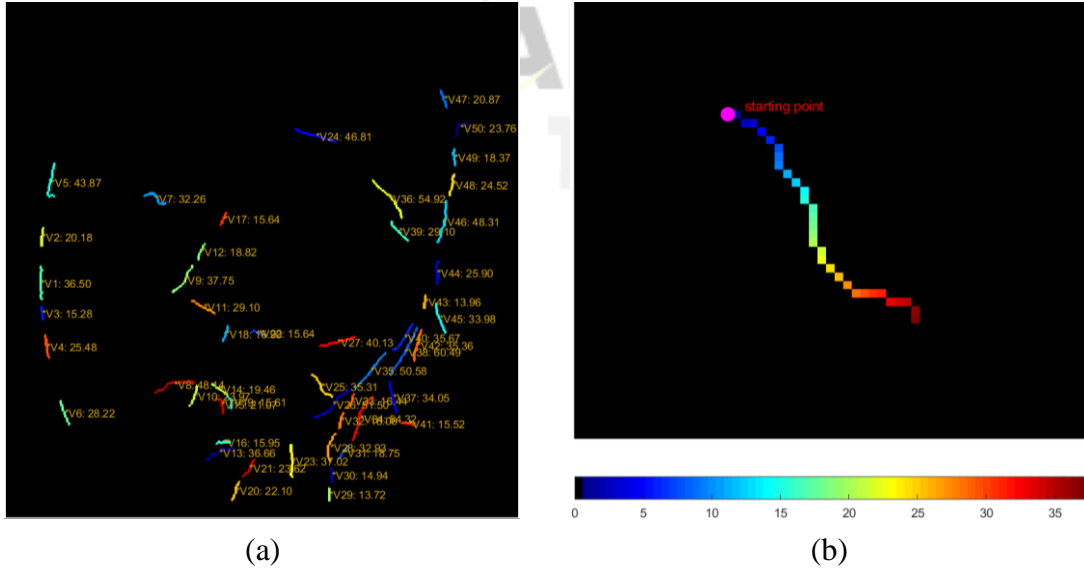


Figure 18. (a) Length of vessel segments using perimeter and (b) color map of geodesic distance transform.

### 3.4 Tortuosity and Width of Vessels Segments

A Retinal blood vessels for developed retina are generally straight or to some extent

and gradually curved. However, retinal vascular diseases can effect tortuosity in its structure, defined as a non-smooth appearance of the vessel course or property of a vessel being tortuous. Tortuosity might affect to a small region of a vessel structure or involve the entire retinal vascular tree. For finding the tortuous vessels in ROP images tortuosity was computed for every vessel segment for this element wise division was done between path lengths and distance for vessel segments. We even added a critical value of 1.2 and highlighted the highly tortuous vessels (matter of concern) in images above the critical value. The value 1.2 is just taken as a random value for the experiment the ophthalmologists can decide on a particular value above which they highly tortuous vessels will be highlighted in the image.

Accurate measurement of vessel diameters on retinal images plays an important part in diagnosing retinal diseases. For width measurement in ROP images we used the vessel segmented image and centerline of vessel image and removed the shorter segments in both of them after which they were overlayed. Labelling was performed on both the set of images and then those labelled were matched. If all the labelled match then we compute the width else we matched the selected labels manually and width was computed. For every vessel segment Euclidean distance transform [42] was computed. For each pixel in the image. The distance transform assigns a number that is the distance between that pixel and the nearest nonzero pixel of image. Figure 19 shows the width calculation for vessel 25 in image which came out to be 3.10 pixels.

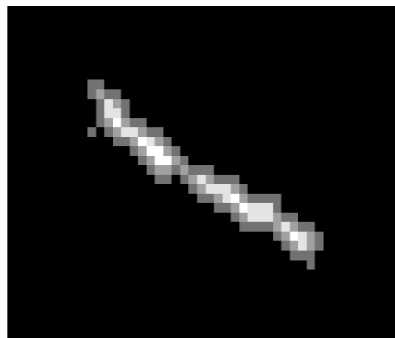


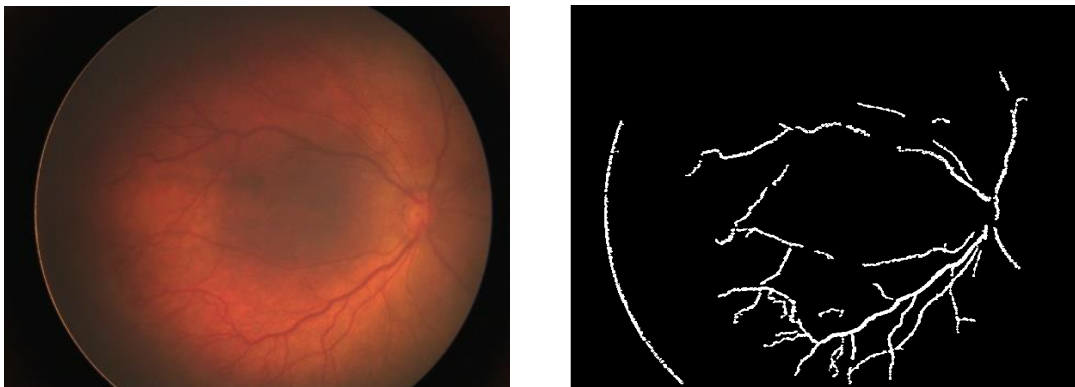
Figure 19. Width calculation using distance transform for vessel segment.

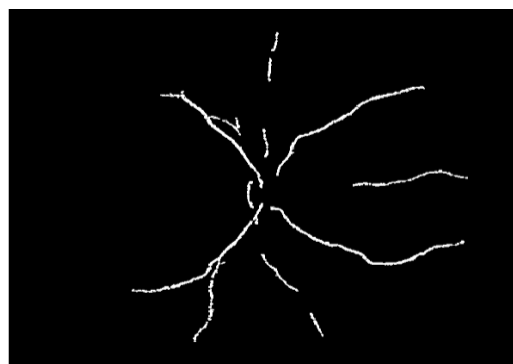
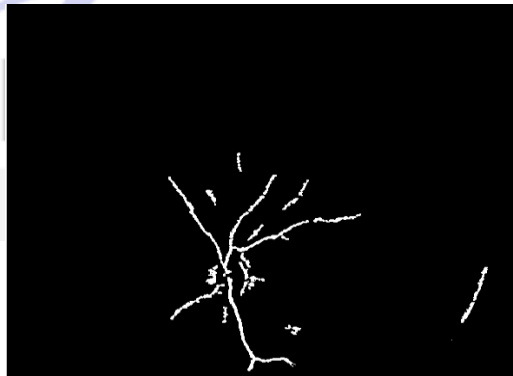
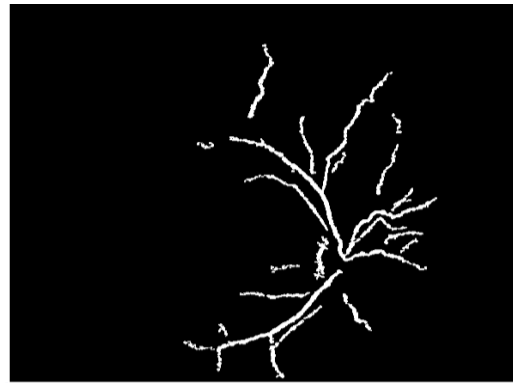
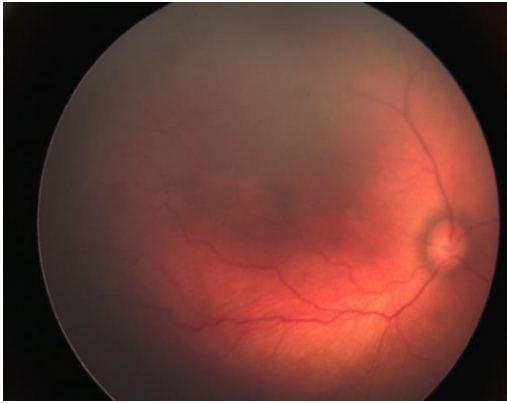
## Chapter 4 Experimental Results and Discussion

This section presents the result following the methods of the previous chapter mentioned as well as show the analysis of results. Sec. 4.1 shows the result of retinal vessel segmentation. Sec. 4.2 shows the length, width and tortuosity measurement results.

### 4.1 Retinal Vessel Segmentation Results

Figure 20 shows the retinal vessel segmentation results for seven images used in this experiment. The proposed algorithm segmented most of vessels in the retinal images. Because of noise the missing pixels in vessel segments can be seen in segmented results and very thin vessels at the end were not segmented clearly. Also due to reflection present in image because of camera limited capabilities even after removing the outer ring the reflection was segmented in few images. Therefore, we can learn from other excellent segmentation methods for improving the original image quality before segmentation to improve preprocessing and finally achieve the better vessel segmentation results.





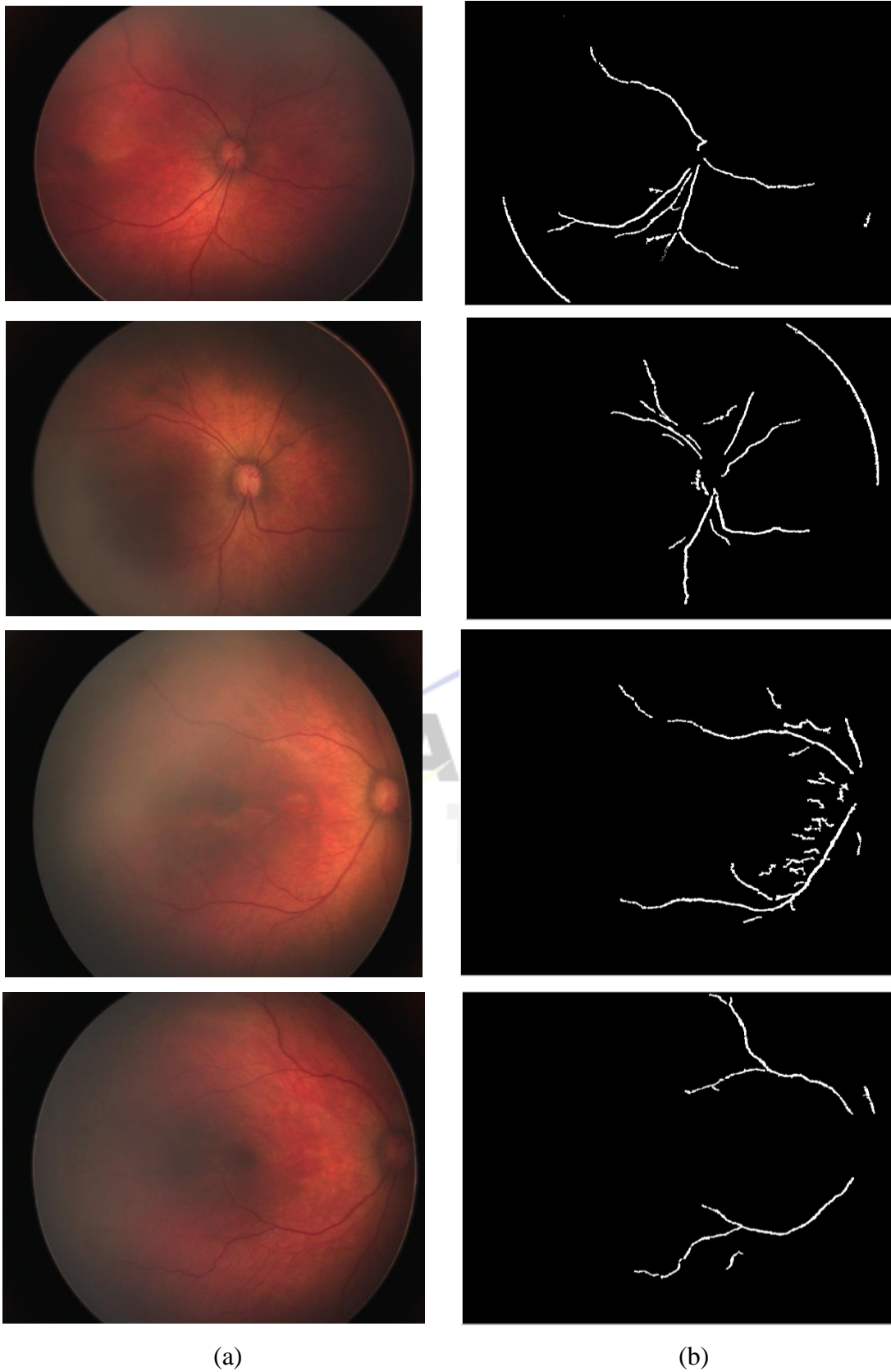


Figure 20. (a) Input images and (b) vessel segmented images using proposed algorithm.

Figure 21 shows retinal vessel segmentation result for image 1 and comparison with

Coye [15] algorithm. The T.L. coye algorithm which works well on retinal blood vessel segmentation for developed retinal images failed to segment out the vessels in ROP image. One of possible reason for this is due to the fact of noise and illumination issues present in the image another possible reason is [15] algorithm was trained and tested on DRIVE dataset which had only developed retinal images with better contrast and quality which our dataset lacked. For most of the ROP images in our dataset coye algorithm failed to segment out the retinal vessels while ours segmented out vessels with missing pixel issue. Therefore, we can learn from other segmentation methods for initial preprocessing of images to make it somewhat near closer to developed retinal images quality before segmentation to achieve the better results.

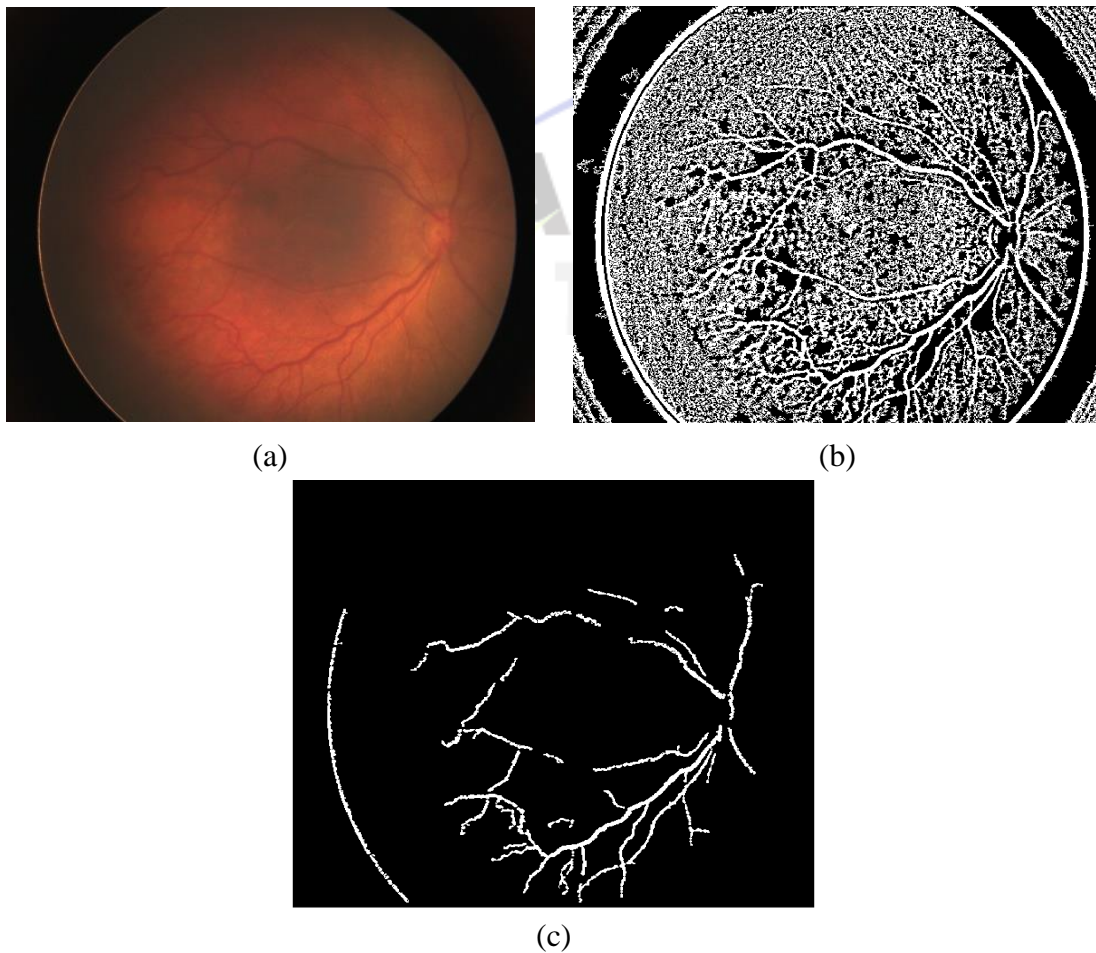


Figure 21. (a) Input image, (b) T. L. Coye segmented image, and (c) Proposed method segmented image.

## 4.2 Branching Point Identification Results

Figure 22 shows the branching point results. Although, it was found that there are certain set of missing pixel regions which were misclassified as endpoints all the branching points were detected successfully. The overlay visualizations helps in identification of branching points and missing pixel positions which are also misclassified as branching points.

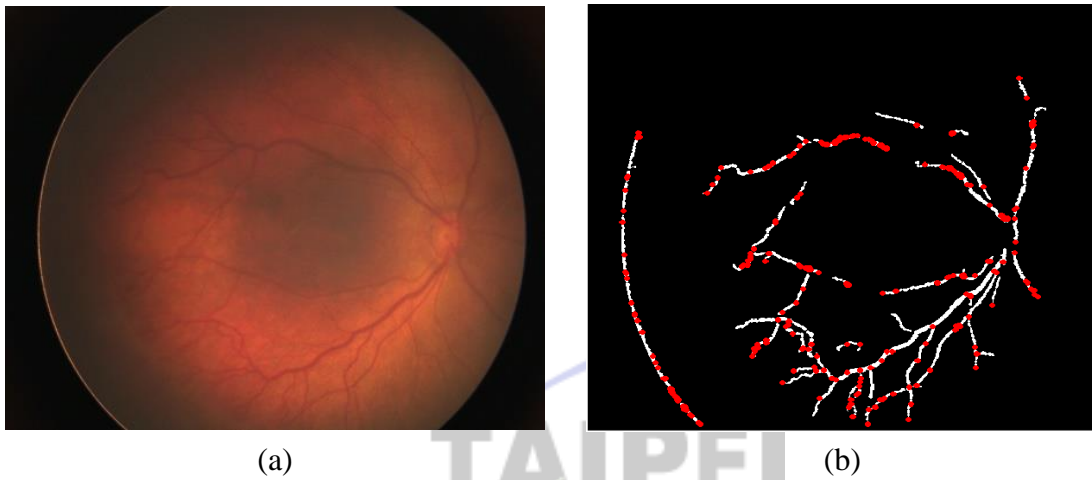


Figure 22. (a) Input image and (b) branching points identified image.

## 4.3 Length, Width and Tortuosity Measurement

### Results

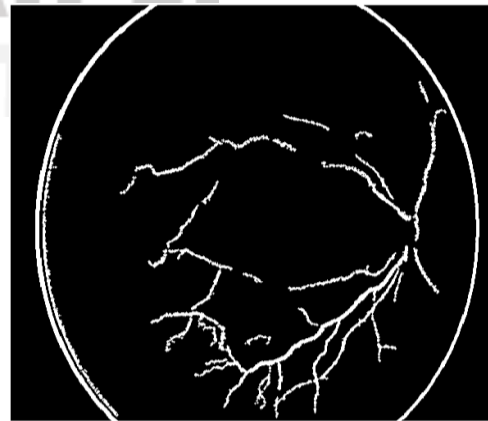
In this section the input fundus images and their corresponding clean vessel images, vessel segmented images with vessel numbers marked on them, length and tortuosity of vessel segments are shown in images. The width of vessel segments are mentioned on the tables for every vessel. The tables consist of total length of every vessel and average width at the end. There are seven images shown in this experiment for measurement results. The results shown in table for length and width detection are according to vessel number marked and their segments. Blood vessels which are originating from the optic disc in fundus images are taken in account for measurements. The branches and branching points of vessels are not included in measuring the length and width for a particular vessel. For



vessels which are curved have been divided into maximum linear segments through the proposed method and then their measurements are done. The vessel segments are labelled automatically and are marked on length and tortuosity measurement images. For each image we have taken four vessels originating from the optic disc as base vessels it is do because from figure 20 (b) we observed most of premature retinal images have mainly four vessels originating from optic disc also these vessels are numbered on vessel segmented images which are marked. The measurement unit of both the length and width of vessels are taken into pixels. The length and width measurements are for each vessel is separately mentioned in tables with the vessels segments of that particular vessel. At bottom of every table the total length of a particular vessel and average width of that vessel is calculated. The rest of chapter 4 shows the complete result of our experiment, including the vessels numbers and measurement results for geometrical physical characteristics of retinal vessels for ROP. The results for image 1 are as follows:



(a)



(b)



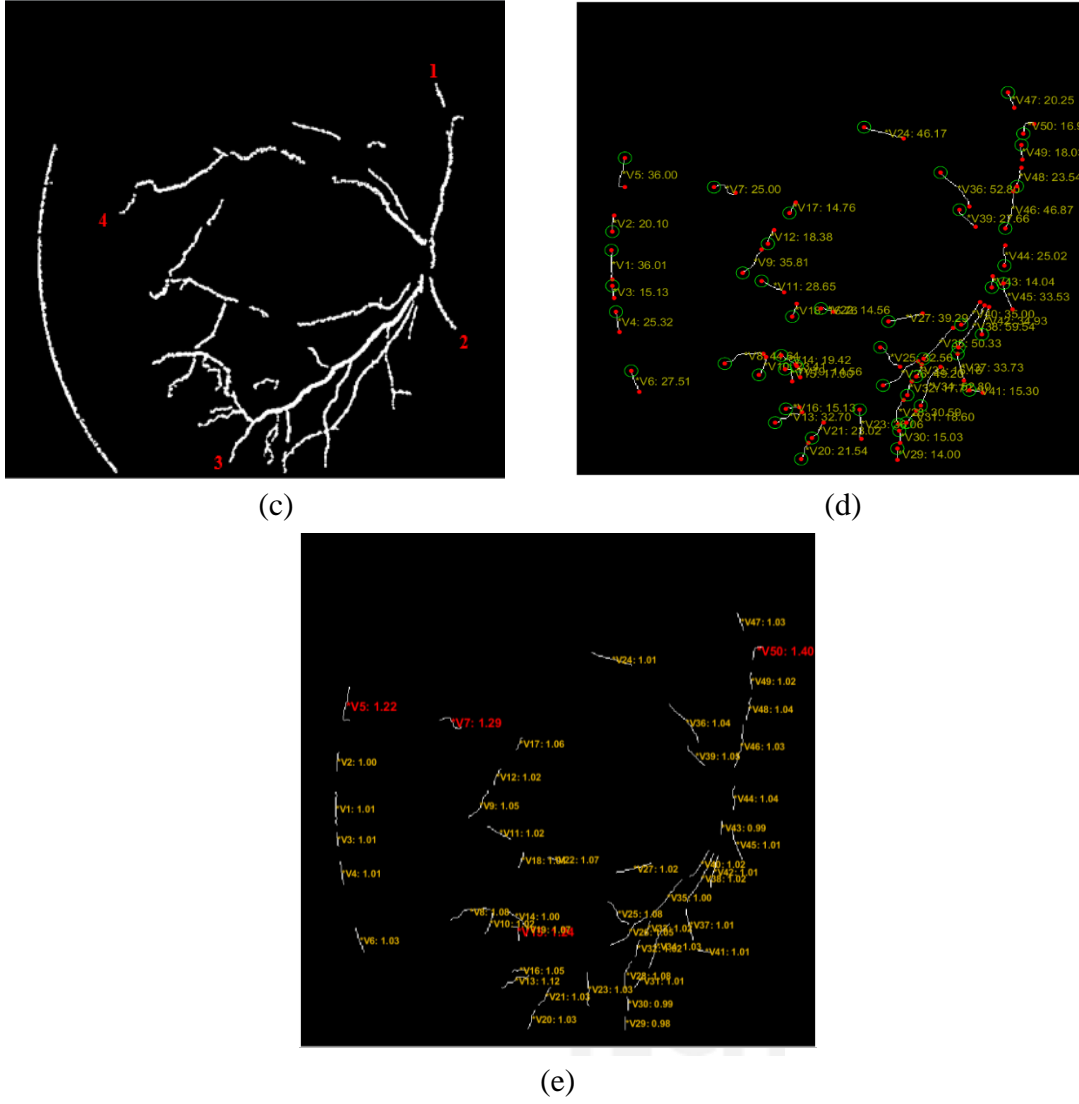


Figure 23. (a) Input image 1, (b) clean vessel image, (c) vessel segmented image with vessel labelled, (d) length of vessel segments using geodesic distance transform, and (e) tortuosity of vessel segments.

Table 2. Represents the length and width of vessel one for image 1.

Vessel No.	Segment	Length (Pixels)	Width (Pixels)
1	V44	20.25	3.50
	V46	16.90	3.50
	V47	18.03	2.80
	V48	23.54	3.31
	V49	46.87	3.30
	V50	25.02	3.10
Total length and average width		150.61	3.20

Table 3. Represents the length and width of vessel two for image 1.

Vessel No.	Segment	Length (Pixels)	Width (Pixels)
2	V45	33.53	3.20

Table 4. Represents the length and width of vessel three for image 1.

Vessel No.	Segment	Length (Pixels)	Width (Pixels)
3	V20	21.54	2.60
	V21	23.02	2.60
	V26	49.20	2.80
	V35	50.33	3.50
	V40	35.00	3.70
Total length and average width		179.09	3.04

From the results from tables 1-3 it is to be noted that these are lengths calculated for the segmented vessels from input fundus image. The actual length of vessels are longer than calculated one. The calculated length excludes the missing pixel regions, discarded shorter segments and thin vessels which were not detected. The process remained the same for rest of images. The vessel 4 in figure 20 (c) was discarded and length was not computed for that because large regions of missing pixels and wrong identification of those as branching points similar with figure 22 (c). The vessel segment labelling was done automatically using the labelling technique mentioned in chapter 3 that is why the labelling of vessel segments in some tables are not in increasing order but are synchronized according to vessels segments in figure 21 (d) and in some images we put the segments in increasing order. The length of three vessels in image1 came out to be 150.61, 33.53 and 179.09 pixels with average width of 3.20, 3.20 and 3.04 pixels respectively. The rest of images used for experiment followed the same procedure for measurement of geometrical physical characteristics of retinal vessels.

The results for image 2 are as follows:

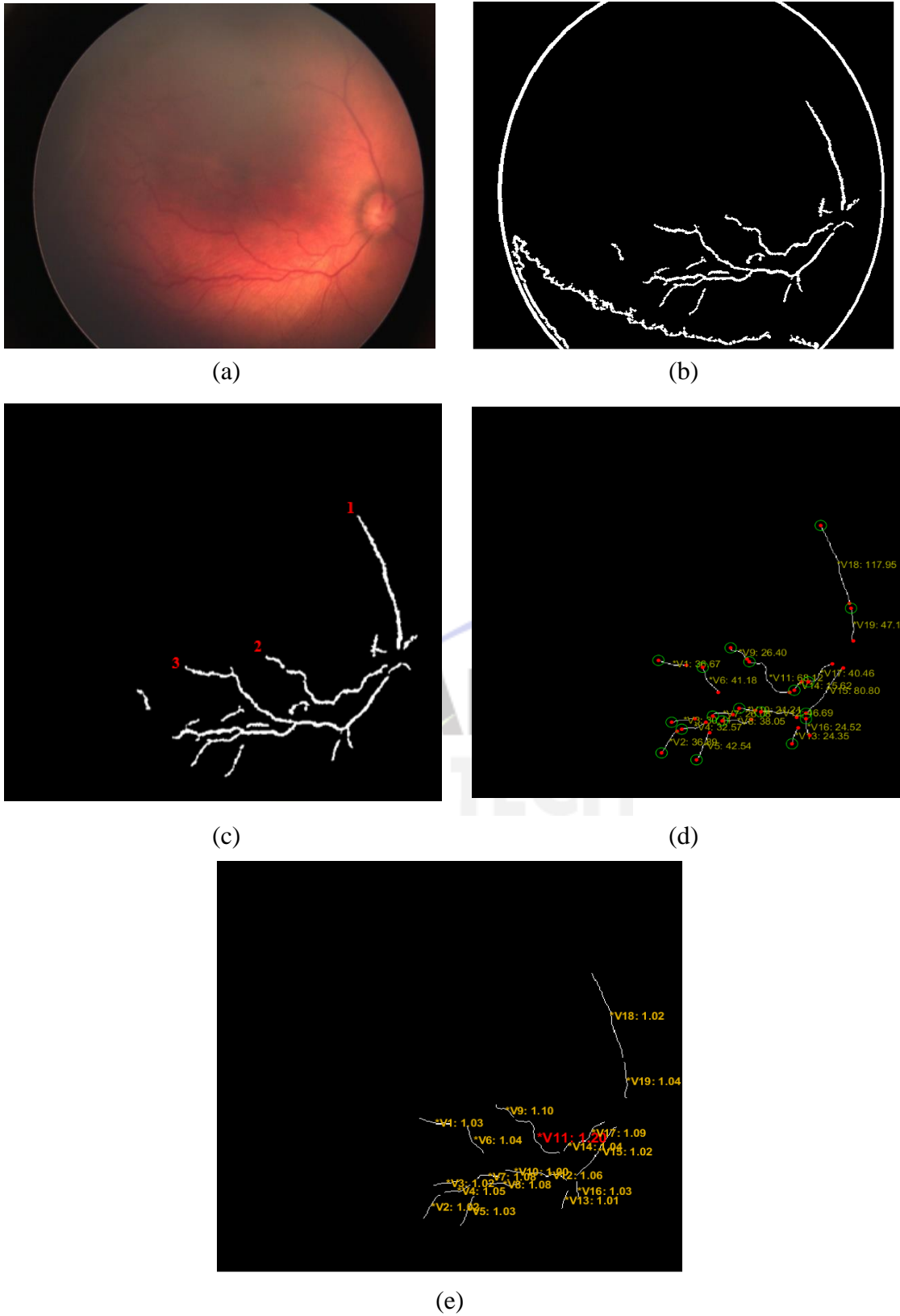


Figure 24. (a) Input image 2, (b) clean vessel image, (c) vessel segmented image with vessel labelled, (d) length of vessel segments using geodesic distance transform, and (e) tortuosity of vessel segments.

Table 5. Represents the length and width of vessel one for image 2.

Vessel No.	Segment	Length (Pixels)	Width (Pixels)
1	V18	117.95	2.60
	V19	47.10	2.60
Total length and average width		165.05	2.60

Table 6. Represents the length and width of vessel two for image2.

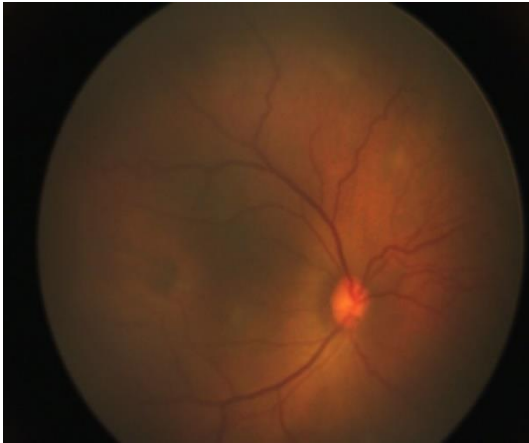
Vessel No.	Segment	Length (Pixels)	Width (Pixels)
2	V9	26.40	2.20
	V11	68.12	2.20
	V14	15.62	2.00
	V17	40.46	2.00
Total length and average width		152.60	2.10

Table 7. Represents the length and width of vessel three for image2.

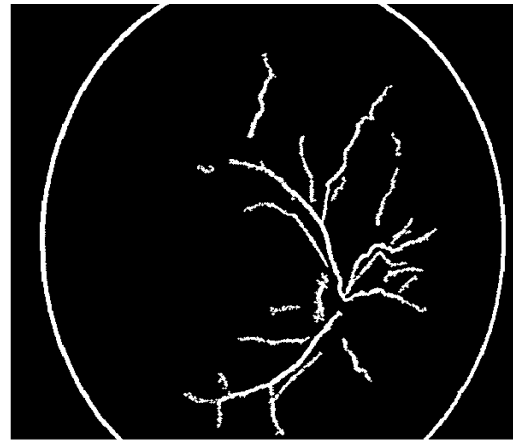
Vessel No.	Segment	Length (Pixels)	Width (Pixels)
3	V1	36.67	2.60
	V6	41.18	2.60
	V10	21.21	2.50
	V12	46.69	2.50
	V15	80.80	2.42
Total length and average width		226.55	2.52

Only three main vessels were segmented from image2. The length of three vessels in image2 came out to be 165.05, 152.60 and 226.55 pixels with average width of 2.60, 2.10 and 2.52 pixels respectively.

The results for image 3 are as follows:



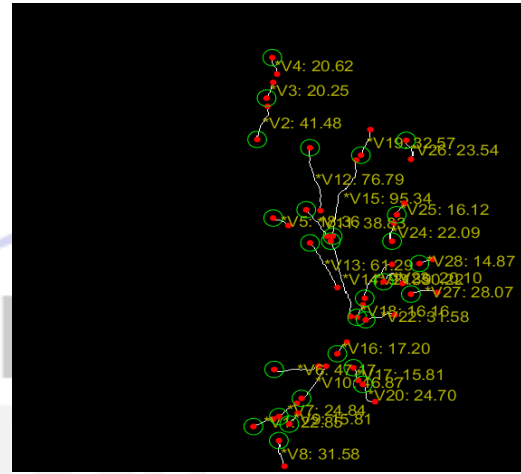
(a)



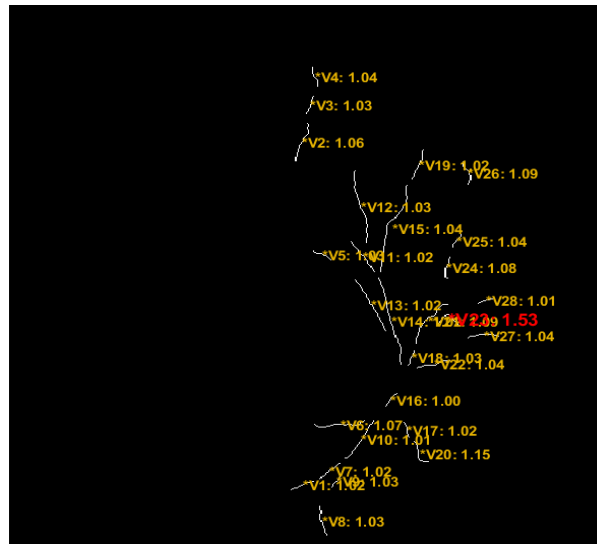
(b)



(c)



(d)



(e)

Figure 25. (a) Input image 3, (b) clean vessel image, (c) vessel segmented image with vessel labelled, (d) length of vessel segments using geodesic distance

transform, and (e) tortuosity of vessel segments.

Table 8. Represents the length and width of vessel one for image 3.

Vessel No.	Segment	Length (Pixels)	Width (Pixels)
1	V11	38.33	4.90
	V14	93.39	4.90
Total length and average width		165.05	4.90

Table 9. Represents the length and width of vessel two for image 3.

Vessel No.	Segment	Length (Pixels)	Width (Pixels)
2	V18	16.16	3.80
	V21	50.22	3.80
	V28	14.87	2.80
Total length and average width		81.25	3.46

Table 10. Represents the length and width of vessel three for image 3.

Vessel No.	Segment	Length (Pixels)	Width (Pixels)
3	V2	31.58	2.80

Table 11. Represents the length and width of vessel four for image 3.

Vessel No.	Segment	Length (Pixels)	Width (Pixels)
4	V1	22.85	3.24
	V7	24.84	3.24
	V10	46.87	3.80
	V16	17.20	4.20
Total length and average width		111.76	3.62

All four vessels were segmented from image3. The length of three vessels in image3 came out to be 165.05, 81.25, 31.58 and 111.76 pixels with average width of 4.90, 3.46, 2.80 and 3.62 pixels respectively.

The results for image 4 are as follows:

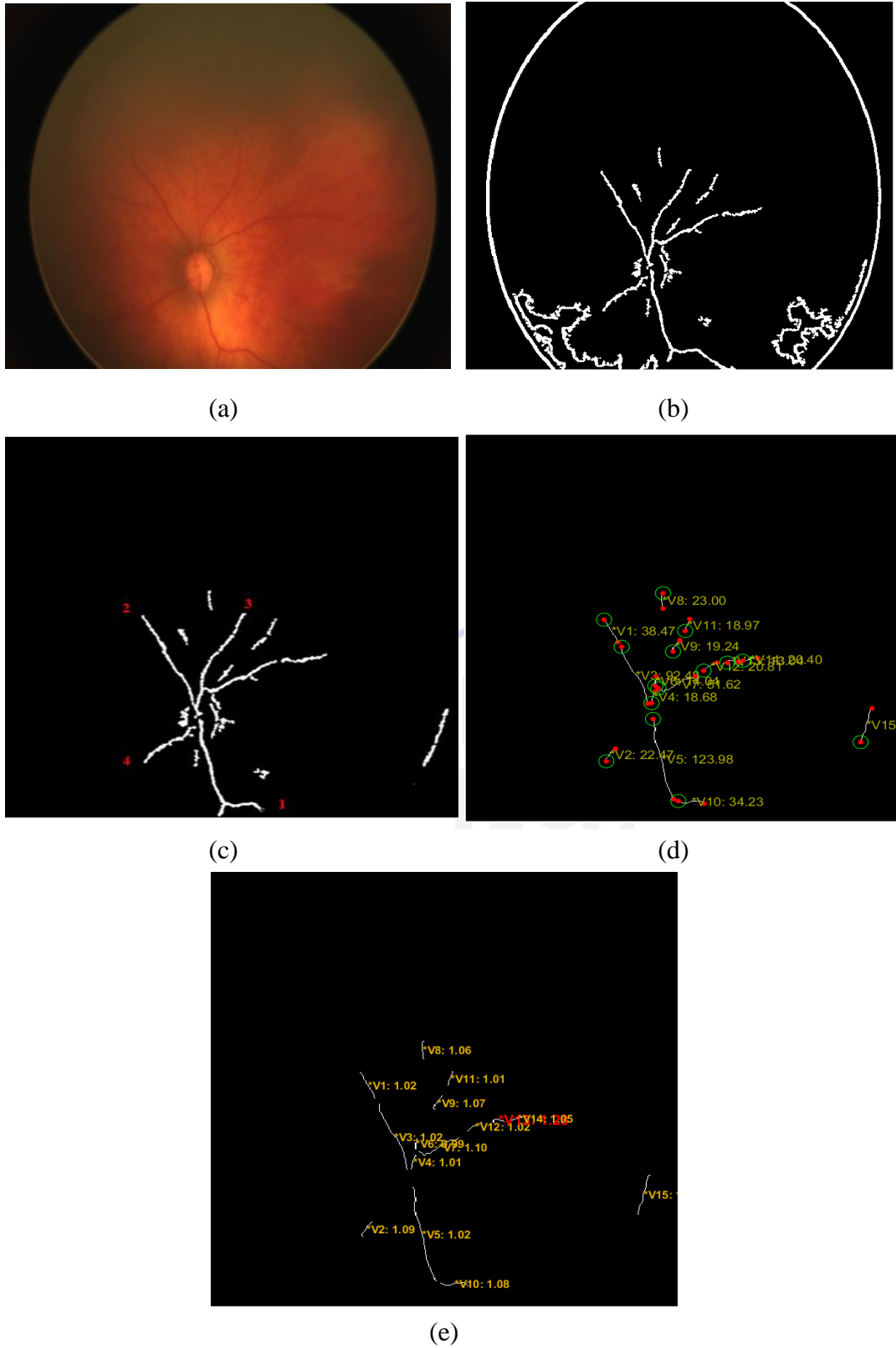


Figure 26. (a) Input image 4, (b) clean vessel image, (c) vessel segmented image with vessel labelled, (d) length of vessel segments using geodesic distance transform, and (e) tortuosity of vessel segments.

Table 12. Represents the length and width of vessel one for image 4.

Vessel No.	Segment	Length (Pixels)	Width (Pixels)
1	V5	123.98	2.50
	V10	34.23	2.50
Total length and average width		158.21	2.50

Table 13. Represents the length and width of vessel two for image 4.

Vessel No.	Segment	Length (Pixels)	Width (Pixels)
2	V1	38.47	2.40
	V3	92.48	2.42
Total length and average width		130.95	2.41

Table 14. Represents the length and width of vessel three for image 4.

Vessel No.	Segment	Length (Pixels)	Width (Pixels)
3	V4	18.68	2.30
	V6	14.04	2.30
	V9	19.24	2.20
	V11	18.97	2.00
Total length and average width		70.93	2.20

Table 15. Represents the length and width of vessel four for image 4.

Vessel No.	Segment	Length (Pixels)	Width (Pixels)
4	V2	22.47	2.20

All the four vessels were segmented for image4 originating from the optic disc.

The length of four vessels in image3 came out to be 158.21, 130.95, 70.93 and 22.47 pixels with average width of 2.50, 2.41, 2.20 and 2.20 pixels respectively. Similarly, the length and width for image 4-7 were computed and mentioned in tables below.



The results for image 5 are as follows:

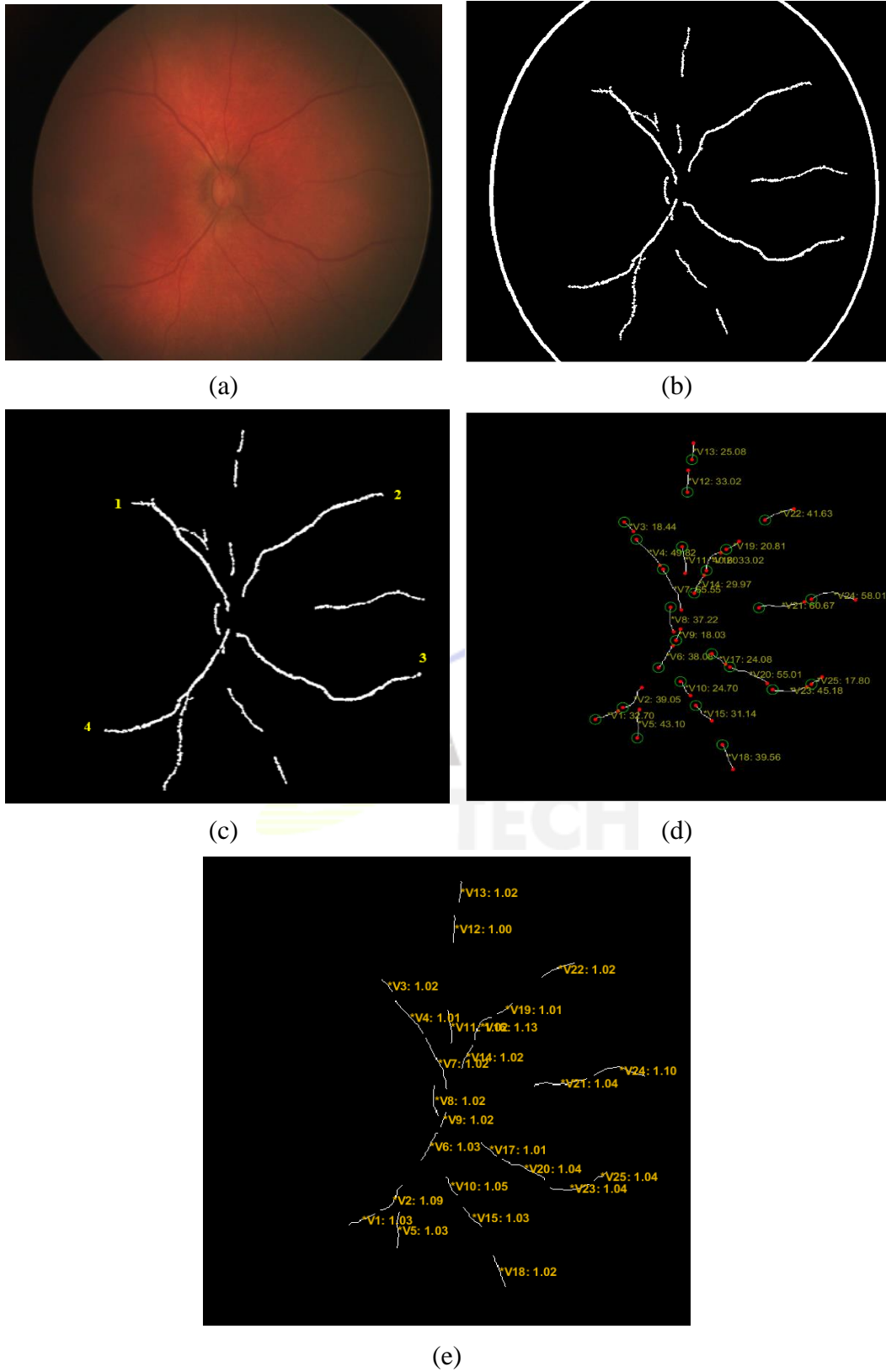


Figure 27. (a) Input image 5, (b) clean vessel image, (c) vessel segmented image with vessel labelled, (d) length of vessel segments using geodesic distance transform, and (e) tortuosity of vessel segments.

Table 16. Represents the length and width of vessel one for image 5.

Vessel No.	Segment	Length (Pixels)	Width (Pixels)
1	V3	18.44	3.40
	V4	49.82	3.60
	V7	65.55	3.60
Total length and average width		81.25	3.50

Table 17. Represents the length and width of vessel two for image 5.

Vessel No.	Segment	Length (Pixels)	Width (Pixels)
2	V14	29.97	3.40
	V16	33.02	3.42
	V19	20.81	3.60
	V22	41.63	3.60
Total length and average width		125.43	3.50

Table 18. Represents the length and width of vessel three for image 5.

Vessel No.	Segment	Length (Pixels)	Width (Pixels)
3	V17	24.08	3.50
	V20	55.10	3.50
	V23	45.18	3.40
	V25	17.80	3.40
Total length and average width		142.07	3.45

Table 19. Represents the length and width of vessel four for image 5.

Vessel No.	Segment	Length (Pixels)	Width (Pixels)
4	V1	32.70	3.24
	V2	39.05	3.40
	V6	38.08	3.50
	V9	18.03	3.50
Total length and average width		127.23	3.41

The length of four vessels in image5 came out to be 81.25, 125.43, 143.07 and 127.23 pixels with average width of 3.50, 3.50, 3.45 and 3.41 pixels respectively.

The results for image 6 are as follows:

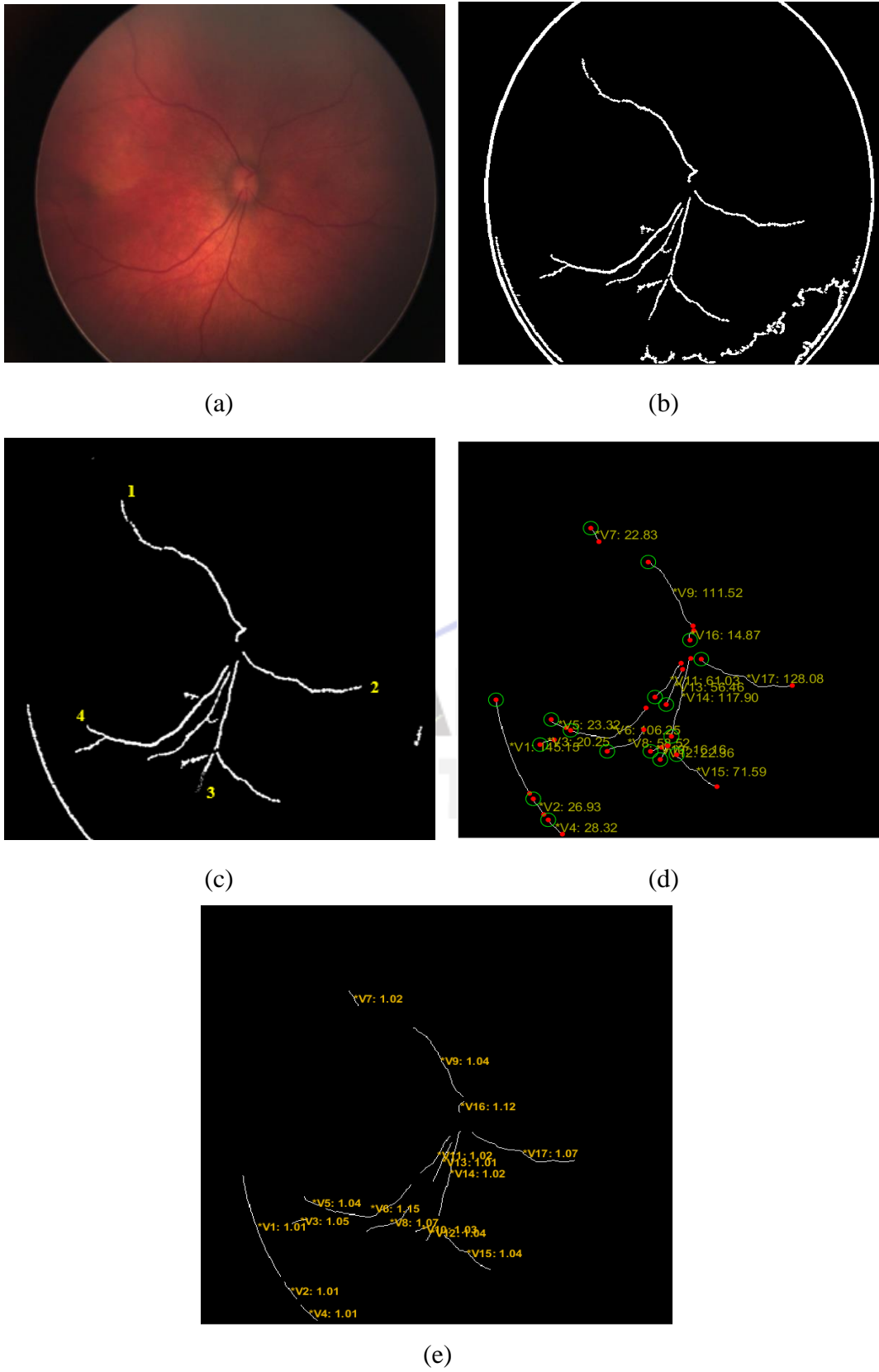


Figure 28. (a) Input image 6, (b) clean vessel image, (c) vessel segmented image with vessel labelled, (d) length of vessel segments using geodesic distance

transform, and (e) tortuosity of vessel segments.

Table 20. Represents the length and width of vessel one for image 6.

Vessel No.	Segment	Length (Pixels)	Width (Pixels)
1	V7	22.83	3.50
	V9	111.52	3.50
	V16	14.87	3.80
Total length and average width		149.20	3.60

Table 21. Represents the length and width of vessel two for image 6.

Vessel No.	Segment	Length (Pixels)	Width (Pixels)
2	V17	128.08	3.50


Table 22. Represents the length and width of vessel three for image 6.

Vessel No.	Segment	Length (Pixels)	Width (Pixels)
3	V12	22.36	3.10
	V14	117.90	3.50
Total length and average width		268.34	3.30

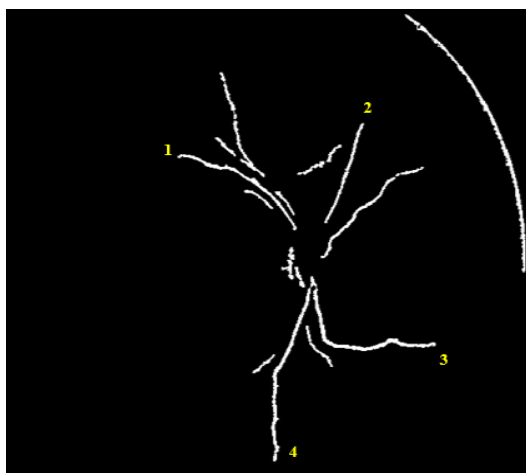
Table 23. Represents the length and width of vessel four for image 6.

Vessel No.	Segment	Length (Pixels)	Width (Pixels)
4	V5	23.32	3.50
	V6	106.25	3.60
	V11	61.03	3.80
Total length and average width		190.60	3.63

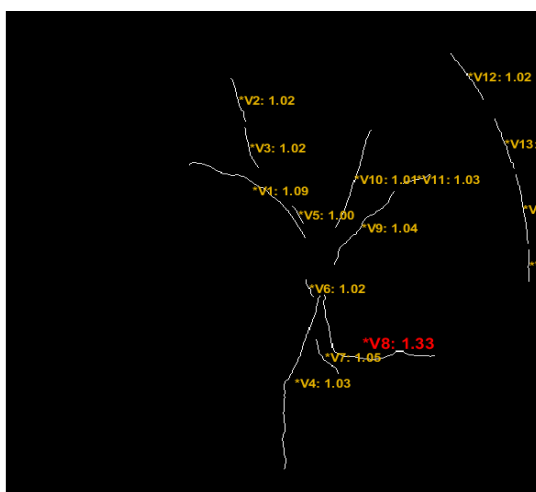
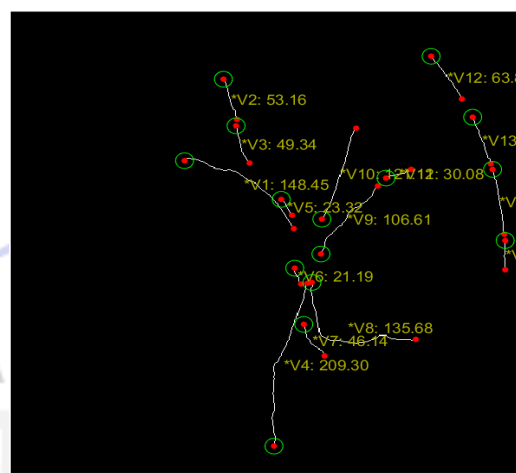
The length of four vessels in image6 came out to be 149.20, 128.08, 268.34 and 190.60 pixels with average width of 3.60, 3.50, 3.30 and 3.63 pixels respectively.



(b)



(d)



(e)

49

Table 24. Represents the length and width of vessel one for image 7.

Vessel No.	Segment	Length (Pixels)	Width (Pixels)
1	V1	148.45	3.42

Table 25. Represents the length and width of vessel two for image 7.

Vessel No.	Segment	Length (Pixels)	Width (Pixels)
2	V10	121.12	3.10

Table 26. Represents the length and width of vessel three for image 7.

Vessel No.	Segment	Length (Pixels)	Width(Pixels)
3	V8	135.68	3.50

Table 27. Represents the length and width of vessel four for image 7.

Vessel No.	Segment	Length (Pixels)	Width (Pixels)
4	V4	209.30	3.60

Image7 results came out to be one of the cleanest segmentation result in our experiment. Although, the very thin vessels present in the end of vessels were not segmented clearly. All the four retinal vessels originating from optic disc were segmented successfully with no missing pixel regions and only the bifurcation points were removed for calculating the length of vessels. The length of four vessels in image7 came out to be 148.45, 121.12, 135.68 and 209.30 pixels with average width of 3.42, 3.10, 3.50 and 3.60 pixels respectively.

The results for image8 are as follows:

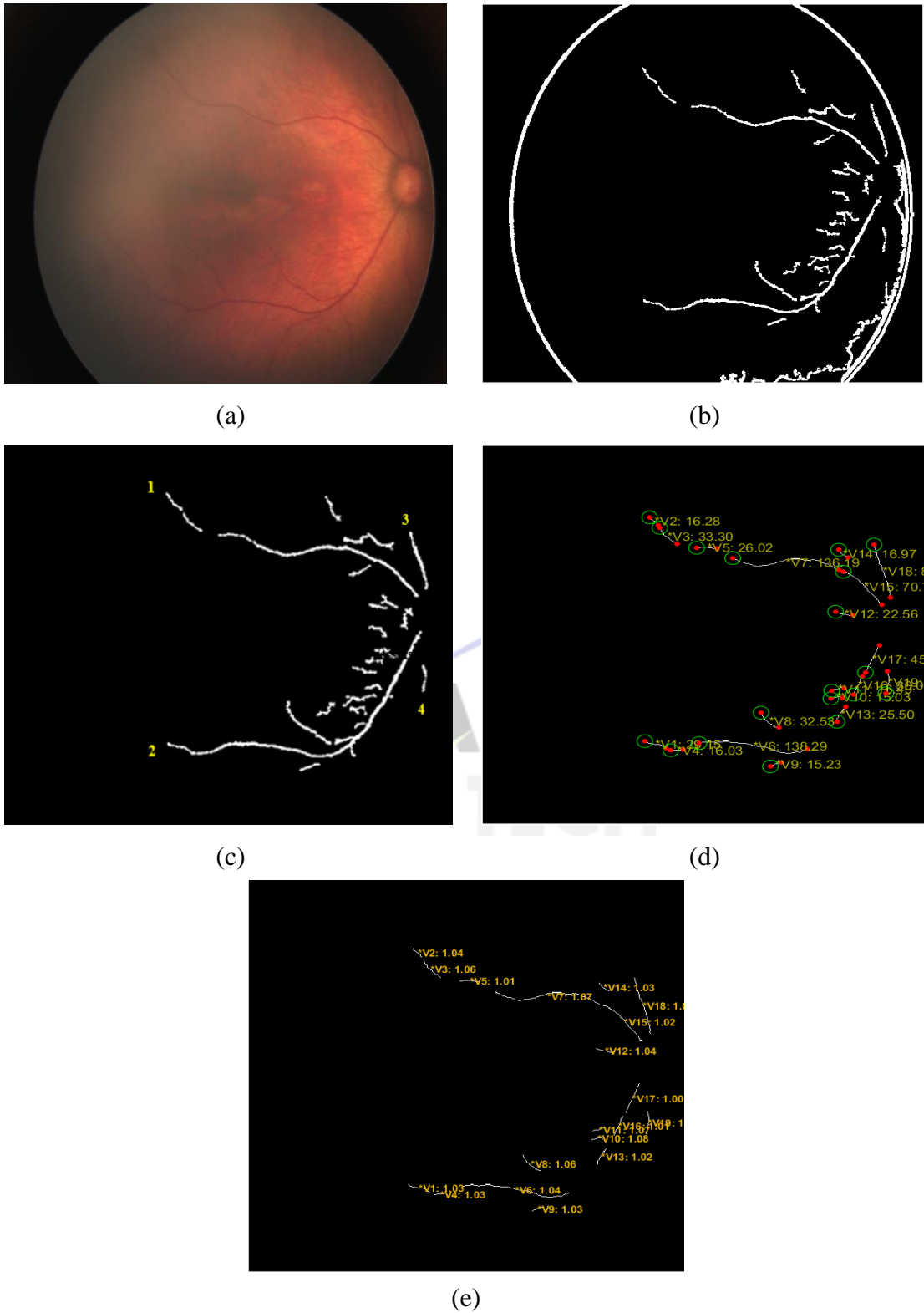


Figure 30. (a) Input image 8, (b) clean vessel image, (c) vessel segmented image with vessel labelled, (d) length of vessel segments using geodesic distance transform, and (e) tortuosity of vessel segments.

Table 28. Represents the length and width of vessel four for image 8.

Vessel No.	Segment	Length (Pixels)	Width (Pixels)
1	V15	23.32	3.80
	V7	106.25	3.60
	V5	26.02	3.62
	V3	136.19	3.42
	V2	70.72	3.20
Total length and average width		362.50	3.52

Table 29. Represents the length and width of vessel four for image 8.

Vessel No.	Segment	Length (Pixels)	Width (Pixels)
2	V17	45.69	3.82
	V16	30.08	3.80
	V13	25.50	3.60
	V6	128.29	3.60
	V4	16.03	3.42
	V1	29.15	3.20
Total length and average width		274.74	3.57

Table 30. Represents the length and width of vessel four for image 8.

Vessel No.	Segment	Length (Pixels)	Width (Pixels)
3	V18	84.65	2.80

Table 31. Represents the length and width of vessel four for image 8.

Vessel No.	Segment	Length (Pixels)	Width (Pixels)
4	V19	34.06	2.80

The length of four vessels in image8 came out to be 326.50, 274.74, 84.65 and 34.06 pixels with average width of 3.52, 3.57, 2.80 and 2.80 pixels respectively.



The results for image 9 are as follows:

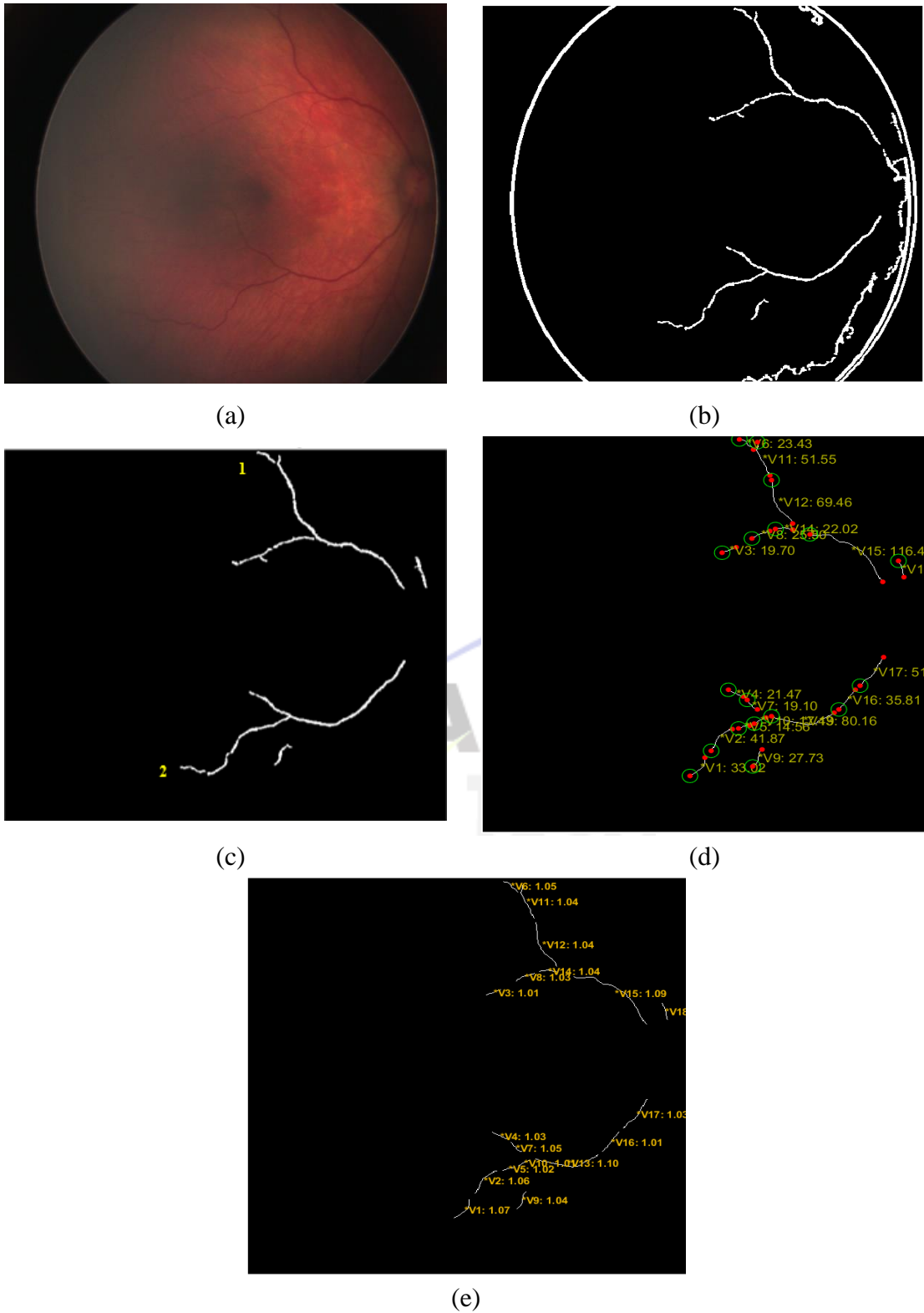


Figure 31. (a) Input image 9, (b) clean vessel image, (c) vessel segmented image with vessel labelled, (d) length of vessel segments using geodesic distance transform, and (e) tortuosity of vessel segments.

Table 32. Represents the length and width of vessel one for image 9.

Vessel No.	Segment	Length (Pixels)	Width (Pixels)
1	V15	116.40	4.80
	V12	69.46	4.82
	V11	51.55	4.80
Total length and average width		237.41	4.80

Table 33. Represents the length and width of vessel two for image 9.

Vessel No.	Segment	Length (Pixels)	Width (Pixels)
2	V17	51.61	4.82
	V16	35.81	4.80
	V13	80.16	4.60
	V10	17.49	3.80
	V5	14.56	3.41
	V2	41.87	3.20
	V1	33.02	3.20
Total length and average width		274.52	3.97

The length of two vessels in image9 came out to be 237.41 and 274.52 pixels with average width of 4.80 and 3.97 pixels respectively.

# Chapter 5 Conclusions and Future Work

This chapter gives the conclusion and future research. Section 5.1 gives the conclusion of the research and section 5.2 gives the direction of future research.

## 5.1 Conclusions

This thesis includes data which is of premature infants possessing retinopathy of prematurity. As for now with the available diagnostic tools and less awareness of this disease the premature infants face the problem of untimely treatment and as a result to irreversible blindness at early age. The retinal vessel segmentation is a tough task most of the methods are tested on publically available datasets which are of developed retina. These images in the publically available datasets are already preprocessed and have better contrast and almost less or no noise. The data used in this study showed that the existing method for segmentation failed while our method was able to segment out retinal vessels on ROP images. We strived to provide a simple yet powerful diagnostic tool which segmented out most of retinal vessels in premature images as well as delineate the geometrical physical characteristics of retinal vessels like length, width and tortuosity of retinal blood vessels in ROP images.

According to the experimental results, our retinal vessel segmentation results showed an effective and easy way to reduce the noise present in retinal images and enhance the contrast. Methods such as background noise removal, morphological opening using specific channel and removing smaller segments lead to a clear network of retinal blood vessels in premature infant eye images. Incorporating these techniques yielded a better and effective image processing method for better segmentation of retinal images with ROP. For length detection two method were tried and tested from which geodesic distance transform algorithm was used for calculating the approximate length of vessels as it gave more precise length results then other method. Our method for width calculation

leads to cross checking of automatic labelling of vessel segments and distance transformation used lead to precise calculation for vessels diameter. Tortuosity of vessel segments were also calculated separately for every vessel segment and vessels with high tortuosity can be marked easily. All together it becomes an accommodating tool for ophthalmologist for finding the approximate measurements of the retinal blood vessels and reduce the probability of blindness occurrence in infants by making better decisions on right time.

## **5.2 Future Work**

An ophthalmologist espouse visual judgement from a retinal fundus image. These judgments are based on limits of what's humans eye can perceive. AI models and tools have proven their efficiency in overcoming problems and capability of determining parameters for clinical definitions. This study also has limitations which we will try to overcome. We will try to add initial preprocessing steps before segmentation of retinal blood vessels for noise and illumination issues present in premature retinal fundus images also to improve the contrast and to clean the fundus image.

The branching points in in retinal blood vessels play an important role in this study the model was incapable in identifying the missing regions and consider them as end points. This problem can also be dealt with improving the segmentation results and enhancing models capability in distinguishing bifurcation and missing pixels regions which can lead to generation of automatic process for precise delineation of vessel characteristics.

## References

- [1] T. Aaberg, I. Ben-Sira, S. Charles, J. Clarkson, B. Z. Cohen, J. Flynn, R. Foos, A. Garner, T. Hirose, F. Koerner, R. Machemer, A. Majima, A. McCormick, A. McPherson, H. Paulmann, G. Quinn, J. Robertson, Y. Tanaka, W. Tasman, T. Topping, and Michael Trese, “An international classification of retinopathy of prematurity: II the classification of retinal detachment” *Arch. of Ophthalmology*, vol. 105, no. 7, pp.906-912, Jul. 1987.
- [2] S. N. Harrell and D. Brandon, “Retinopathy of prematurity: The disease process, classifications, screening, treatment, and outcomes,” *Neonatal Network*, vol. 26, no. 6, pp. 371–378, Dec. 2007.
- [3] A. Hellstrom, L. E. H. Smith, and O. Dammann, “Retinopathy of prematurity,” *The Lancet*, vol. 382, no. 9902, pp. 1445–1457, Jul. 2013.
- [4] American Association for Pediatric Ophthalmology & Strabismus, *Retinopathy of Prematurity*, American Association for Pediatric Ophthalmology & Strabismus, Beach street, San Francisco, CA, July 04, 2020. Accessed on: Feb. 20, 2021. [Online]. Available: <https://aapos.org/glossary/retinopathy-of-prematurity>.
- [5] A. M. Freitas, R. Mörschbacher, M. R. Thorell, and E. L. Rhoden, “Incidence and risk factors for retinopathy of prematurity: a retrospective cohort study,” *International Journal of Retina and Vitreous*, vol. 4, no. 1, pp.1–8, May 2018.
- [6] F. P. Vidal, F. Bello, K. W. Brodlie, N. W. John, D. Gould, R. Phillips, and N. J. Avis, “Principles and applications of computer graphics in medicine,” *Computer Graphics Forum*, vol. 25, No. 1, pp.113-137, Mar. 2006.
- [7] C. L. Srinidhi, P. Aparna, and J. Rajan, “Recent advancements in retinal vessel

- segmentation,” *Journal of medical systems*, vol. 4, pp.70-91, Apr. 2017.
- [8] M. M. Fraz, S. A. Barman, P. Remagnino, A. Hoppe, A. Basit, B. Uyyanonvara, A. R. Rudnicka, and C. G. Owen, “An approach to localize the retinal blood vessels using bit planes and centerline detection,” *Computer Methods and Programs in Biomedicine*, vol. 108 no. 2, pp.600-616 Nov. 2012.
- [9] M. M. Fraz, A. Basit, and S. A. Barman, “Application of morphological bit planes in retinal blood vessel extraction,” *Digital Imaging*, vol. 26 no. 2, pp.274–286, Apr. 2013.
- [10] E. M. Sigurðsson, S. Valero, J. A. Benediktsson, J. Chanussot, H. Talbot, and E. Stefánsson, “Automatic retinal vessel extraction based on directional mathematical morphology and fuzzy classification,” *Pattern Recognition Letters*, vol.1, pp.164-171, Oct. 2014.
- [11] E. Imani, M. Javidi, and H. R. Pourreza, “Improvement of retinal blood vessel detection using morphological component analysis,” *Comput. Methods Prog. Biomed.*, vol. 118, no. 3, pp.263–279, Mar. 2015.
- [12] S. Roychowdhury, D. D. Koozekanani, and K. K. Parhi, “Iterative vessel segmentation of fundus images,” *IEEE Trans. Biomed. Engg*, vol. 62, no. 7, pp.1738–1749, Jul. 2015.
- [13] T. Mapayi, S. Viriri, and J.R. Tapamo, “Adaptive thresholding technique for retinal vessel segmentation based on GLCM-energy information,” *Computational and Mathematical Methods in Medicine*, Feb. 2015.
- [14] T. Mapayi, S. Viriri, and J. R. Tapamo, “Comparative study of retinal vessel segmentation based on global thresholding techniques,” *Computational and Mathematical Methods in Medicine*, Feb. 2015.
- [15] T. Coye, “A novel retinal blood vessel segmentation algorithm for fundus

- images,” MATLAB Cent. File Exch., 2016. Accessed on: Feb. 20, 2021.  
[Online].Available:  
<http://www.mathworks.com/matlabcentral/fileexchange/50839>
- [16] P. Furtado, C. Travassos, R. Monteiro, S. Oliveira, C. Baptista, and F. Carrilho, “Segmentation of eye fundus images by density clustering in diabetic retinopathy,” in *Proc. of IEEE EMBS Int. Conf. on Biomedical & Health Informatics (BHI)*, Orlando, FL, pp.25-28, Feb. 2017.
  - [17] T. Intaramanee, S. Rasmequan, K. Chinnasarn, B. Jantarakongkul, and A. Rodtook, “Optic disc detection via blood vessels origin using morphological end point,” in *Proc. of IEEE Int. Conf. on Advanced Informatics: Concepts, Theory And Application (ICAICTA)*, Penang, Malaysia, pp.1-6, Aug. 2016.
  - [18] M. Saranya and A. G. Selvarani, “Fundus Image Screening for Diabetic Retinopathy,” *Indian Journal of Science and Technology*, vol. 9, no. 25, pp.1-6. 2016.
  - [19] S. P. Saponaro, W. Treible, A. Kolagunda, S. Rhein, J. Caplan, C. Kambhamettu, and R. Wisser, “Three-dimensional segmentation of vesicular networks of fungal hyphae in macroscopic microscopy image stacks,” in *Proc. of IEEE Int. Conf. on Image Processing (ICIP)*, pp.3285-3289, Sep. 2017.
  - [20] A. M. R. R. Bandara and P. W. G. R. M. P. B. Giragama, “A retinal image enhancement technique for blood vessel segmentation algorithm,” in *Proc. of IEEE Int. Conf. on Industrial and Information Systems (ICIIS)*, Peradeniya, Sri Lanka, pp.1-5, Feb. 2017.
  - [21] A. Hellström, L. E. Smith, and O. Dammann, “Retinopathy of prematurity,” *The lancet*, vol. 382, no. 9902, pp.1445-1457, Oct. 2013.
  - [22] M. Gandhi and R. Dhanasekaran, “Diagnosis of diabetic retinopathy using

- morphological process and SVM classifier,” in *Proc. of IEEE Int. Conf. on Communication and Signal Processing*, pp. 873-877, Apr. 2013.
- [23] T. Y. Wong and P. Mitchell, “Hypertensive retinopathy,” *New England Journal of Medicine*, vol. 351, no. 22, pp.2310-2317, Nov. 2004.
- [24] S. Y. Kim, S. Sadda, J. Pearlman, M. S. Humayun, E. de Juan Jr, B. M. Melia, and W. R. Green, “Morphometric analysis of the macula in eyes with disciform age-related macular degeneration,” *Retina*, vol. 22, no. 4, pp. 471-477, Aug. 2002.
- [25] E. Grisan, M. Foracchia, and A. Ruggeri, “A novel method for the automatic grading of retinal vessel tortuosity,” *IEEE Trans. on Medical Imaging*, vol. 27, no. 3, pp.310-319, Mar. 2008.
- [26] F. Oloumi, R. M. Rangayyan, and A. L. Ells, “Computer-aided diagnosis of plus disease in retinal fundus images of preterm infants via measurement of vessel tortuosity,” in *Proc. of IEEE 37th Annual Int. Conf. of Engineering in Medicine and Biology Society (EMBC)*, Milan, Italy, pp.4338-4342, Nov. 2015.
- [27] H. Hao, D. K. Kumar, and B. Aliahmad, "Measured vessel length in retinal vessel diameter measurement," in *Proc. of 5<sup>th</sup> ISSNIP-IEEE Biosignals and Biorobotics Conference: Biosignals and Robotics for Better and Safer Living (BRC)*, Salvador, Brazil, pp. 1-5, Aug. 2014.
- [28] D. K. Kumar, B. Aliahmad, and H. Hao, “Retinal vessel diameter measurement using unsupervised linear discriminant analysis,” *ISRN Ophthalmol.*, vol. 6, pp. 151369-151375, Nov. 2012.
- [29] J. Lowell, A. Hunter, D. Steel, A. Basu, R. Ryder, and R. L. Kennedy, “Measurement of retinal vessel widths from fundus images based on 2-D modeling,” *IEEE Trans. on Medical Imaging*, vol. 23, no. 10, pp.1196-1204, Oct.



2004.

- [30] A. Bhuiyan, B. Nath, and K. Ramamohanarao, "Detection and classification of bifurcation and branch points on retinal vascular network," in *Proc. of International Conference on Digital Image Computing Techniques and Applications (DICTA)*, Fremantle, WA, Australia, pp. 1-8, Dec. 2012.
- [31] S. Al Rashaed, "Retinopathy of prematurity - a brief review," *Dr. Sulaiman Al Habib Medical Journal*, vol. 1, pp.58-64, Dec. 2019.
- [32] Jesse Vislisel and Toni Venckus, "Normal fundus – adult," *EyeRounds.org*, Jan. 2014. Accessed on: Feb. 26, 2021. [Online].  
<https://webeye.ophth.uiowa.edu/eyeforum/atlas/LARGE/Normal-fundus-LRG.jpg>
- [33] B. W. Fleck and N. McIntosh, "Retinopathy of prematurity: recent developments," *NeoReviews*, vol. 10, no. 1, pp.20-30, Jan. 2009.
- [34] M. D. Abramoff, M. K. Garvin, and M. Sonka, "Retinal imaging and image analysis," *IEEE reviews in biomedical engineering*, vol. 3, pp.169-208, Dec. 2010.
- [35] U. Ozkava, S. Ozturk, B. Akdemir, and L. Sevfı, "An efficient retinal blood vessel segmentation using morphological operations," in *Proc. of IEEE 2nd International Symposium on Multidisciplinary Studies and Innovative Technologies (ISMSIT)*, Ankara, Turkey, pp.1-7, Oct. 2018.
- [36] S. M. Pizer, E. P. Amburn, J. D. Austin, R. Cromartie, A. Geselowitz, T. Greer, B. ter Haar Romeny, J. B. Zimmerman, and K. Zuiderveld, "Adaptive histogram equalization and its variations," *Computer vision, graphics, and image processing*, vol. 39, pp.355-368, Sep. 1987.
- [37] R. C. Gonzales and R. E. Woods, *Digital Image Processing*, 2nd ed., Prentice

Hall, 2002.

- [38] A. El-Zaart, "Images thresholding using ISODATA technique with gamma distribution," *Pattern Recognition Image Analysis*, vol. 20, no. 1, pp.29–41, Mar. 2010.
- [39] U. Ozkava, S. Ozturk, B. Akdemir, and L. Sevfi, "An efficient retinal blood vessel segmentation using morphological operations," in *Proc. of IEEE 2<sup>nd</sup> International Symposium on Multidisciplinary Studies and Innovative Technologies (ISMSIT)*, Ankara, Turkey, pp.1-7, Oct. 2018.
- [40] Canny John, "A computational approach to edge detection," *IEEE Trans. on Pattern Analysis and Machine Intelligence*, vol. PAMI-8, no. 6, pp. 679-698, Nov. 1986.
- [41] Haralick, Robert M., and Linda G. Shapiro, *Computer and Robot Vision*, volume I, Addison-Wesley, 1992, pp.28-48.
- [42] P. Soille, "*Morphological Image Analysis: Principles and Applications*", 2<sup>nd</sup> Edition, Secaucus, NJ, pp. 219–221, Mar. 2003.
- [43] C. R. Maurer, Rensheng Qi and, V. Raghavan, "A linear time algorithm for computing exact euclidean distance transforms of binary images in arbitrary dimensions," *IEEE Trans. on Pattern Analysis and Machine Intelligence*, vol. 25, no. 2, pp. 265-270, Feb. 2003.